Investigation of the planetary boundary layer using remote sensing and in-situ measurements at the Kleine Scheidegg and at the Jungfraujoch

Master's Thesis

Faculty of Science

University of Bern

presented by:

Christine Ketterer

2011

Supervisors:

Dr. Ernest Weingartner
Laboratory of Atmospheric Chemistry, Paul Scherrer Institut

Co-Supervisors:

Prof. Dr. Margit Schwikowski
Oeschger Centre for Climate Change Research
and
Laboratory of Radiochemistry and Environmental Chemistry, Paul Scherrer Institut

Advisor:

Dr. Paul Zieger, Dr. Nicolas Bukowiecki
Laboratory of Atmospheric Chemistry, Paul Scherrer Institut
Dr. Martine Collaud-Coen
MeteoSwiss, Payerne

Abstract

The troposphere is divided into planetary boundary layer (PBL) and the free troposphere. The planetary boundary layer is the lowest part of the atmosphere and is directly influenced by the Earth's surface. Humans spend most time of their life in the PBL and breathe its air. As most sources of anthropogenic emitted air pollutants are near the Earth's surface, these pollutants are directly emitted into the PBL. Air quality depends on the amount of emitted compounds and also on the characteristics of the PBL, its depth and flow characteristics. The top of the PBL acts as a lid and therefore, the aerosol concentration is much lower in the free troposphere. Aerosols in the free troposphere and in the PBL contribute to the direct and indirect aerosol effect.

CLACE (Cloud and Aerosol Characterization Experiment) campaigns have been initiated to investigate the indirect and direct aerosol effect. The CLACE2010 campaign took place at the Jungfraujoch (3580 m a.s.l.) and at the Kleine Scheidegg (2061 m a.s.l.) in the Bernese Alps from June to August 2010. The Jungfraujoch measurement site is usually in the free troposphere, except in summer where injections of the PBL are measured. It is important to know, when air of the PBL influences the measurements and how the local PBL behaves, especially as not much is known about the PBL in alpine regions. Another issue was a comparison between PBL height derived by the diffusion model COSMO-2 and directly measured by wind profiler and ceilometer.

Remote sensing instruments, wind profiler and ceilometer were installed at the Kleine Scheidegg to investigate the PBL. In this work two algorithms were tested to estimate planetary boundary layer height using the ceilometer. The analyzed planetary boundary layer above Kleine Scheidegg was compared with in-situ aerosol measurements at the Jungfraujoch. To estimate the quality of diffusion models in alpine regions, the PBL height above Kleine Scheidegg was compared with the PBL height of the forecast model COSMO-2 with a resolution of 2.2 km.

The planetary boundary layer height was determined using ceilometer and wind profiler on fair-weather days over the Kleine Scheidegg. The height varied between 600 m and 1600 m above the Kleine Scheidegg. Planetary boundary layer heights derived by ceilometer and wind profiler agreed well, especially under cloud-free conditions. When the planetary boundary layer height exceeded around 2800 m a.s.l. injections of the PBL were transported upwards by slope winds. This was confirmed by the aerosol measurements at the Jungfraujoch. The measured aerosol absorption and scattering coefficients showed an increase within a certain time delay. The result of the comparison between PBL heights derived by COSMO-2 and measured by wind profiler and ceilometer showed, that COSMO-2 cannot be applied to predict the PBL height in alpine regions.

Contents

List of Figures

List of Tables

Nomenclature

α	Extinction coefficient
β	Backscatter coefficient
Γ	Lapse rate
λ	Wavelength
Θ_v	Virtual potential temperature
AL	Aerosol layer
c	Pollutant concentration
$C_n{}^2$	Acoustic refractive index
CBH	Cloud base height
CBL	Convective boundary layer
CCN	Cloud condensation nuclei
CLACE	Cloud and aerosol characterization experiment
COSMO	Consortium for small-scale modeling
CPC	Condensation particle counter
CWT	Continuous wavelet transformation
D	Particle diameter
DMA	Differential mobility analyzer
FFT	Fast fourier transformation
FT	Free troposphere
g	Gravity acceleration
GAW	Global atmosphere watch
JFJ	Jungfraujoch
k	Karman constant
KLS	Kleine Scheidegg
LCL	Lifting condensation level
LIDAR	Light detection and ranging
M	Wind speed
ML	Mixing layer
N	Particle number concentration
Nd:YAG	Neodymium-doped yttrium aluminium garnet
p	Air pressure
P(r)	Backscatter signal intensity
PBL	Planetary boundary layer

q_l ..... Liquid water content
q_v ..... Water vapor specific humidity
r ..... Water vapour mixing ratio
RADAR ..... Radio detection and ranging
RL ..... Residual layer
RMSE ..... Root-mean-square error
SNR ..... Signal to noise ratio
SODAR ..... Sound detection and ranging
SYNALP ..... Schüepp synoptic weather type of the Alps
T ..... Air temperature
T_v ..... Virtual temperature
u* ..... Friction velocity

1 Introduction

Anthropogenic emitted compounds do not only influence the air quality in the planetary boundary layer (PBL), the lower part of the troposphere, and cause health effects (Brunekreef and Holgate, 2002). They also contribute to the anthropogenic climate change. Air quality depends on the quantity of anthropogenic emissions but it also depends on the properties of the PBL, especially its height and flow characteristic. These compounds are transported into the free troposphere, the higher part of the troposphere. The principal components of the greenhouse effect are carbon dioxide, methane, nitrous oxide, halocarbons and ozone (IPCC, 2007). While the greenhouse gases account for a positive radiative forcing, the total indirect and direct aerosol effect on climate, by absorption or scattering and change in cloud properties, is negative (IPCC, 2007), which means cooling.

1.1 Aerosols

Aerosols are fine suspensions of liquid or solid particles in the air, which are directly emitted or formed by gas-to-particle conversion in the atmosphere. Their sources are of natural or anthropogenic origin. Organic aerosols, like spores, pollen, and bacteria are emitted from plants and animals. Size, concentration and chemical composition of aerosols varies strongly. Oceans, emitting sea salt with a diameter of 2-20 µm, are the most important source of natural inorganic particles. Other important sources are forest fires, dust or volcanic ashes. Anthropogenic sources of aerosols are combustion of fuel or biomasses, dust along roads or from tilled land (Wallace and Hobbs, 2006).

One fundamental parameter of an aerosol is the particle diameter (D), which is used to classify aerosols (Seinfeld, 2006):

- nucleation mode: $D < 10\,\mathrm{nm}$
- Aitken mode: $10\,\mathrm{nm} < D < 0.1\,\mu\mathrm{m}$
- accumulation mode: $0.1\,\mu\mathrm{m} < D < 2.5\,\mu\mathrm{m}$
- coarse mode: $D > 2.5\,\mu\mathrm{m}$

The particle diameter of atmospheric aerosols ranges from a few tens of angstroms to several hundred micrometers. In general, particles less than 2.5 µm are referred as fine particles and those greater than 2.5 µm as coarse particles. The particles of the fine and coarse mode differ in their removal techniques, while washout and rainout remove fine particles, coarse particles

sediment. Furthermore, atmospheric aerosols are divided into nucleation, Aitken, accumulation and coarse mode. Particles in the nucleation mode with a size smaller than 10 nm are freshly formed particles from condensation of hot vapors during combustion processes and from nucleation of atmospheric constituents to primary particles. Particles grow by coagulation with larger particles and depending on their size, they belong to Aitken or accumulation mode. The accumulation mode extends from 0.1 to 2.5 µm and includes also hydrometers. Hydrometers form when water vapor condensates on existing particles. Coarse particles, which are mechanically formed, consist of human-made emissions and natural dust particles as wind blown dust, sea spray, volcanoes or plant particles (Seinfeld, 2006).

1.2 Climate sensitivity

Aerosols are one principal component of the radiative forcing of climate change. The figure 1.1 depicts the radiative forcing values relative to the pre-industrial values (1750) with their uncertainties (black lines). The natural radiative forcing triggers a change in net irradiance at the tropopause of $0.12\,\mathrm{Wm^{-2}}$, which is prevailed by the total net anthropogenic radiative forcing, which is responsible for a change in net irradiance at the tropopause of $1.6\,\mathrm{Wm^{-2}}$. The total anthropogenic aerosol radiative forcing causes a change in net irradiance at the tropopause of $-1.2\,\mathrm{Wm^{-2}}$, which offsets a fraction of anthropogenic greenhouse gas emissions, which accounts for a change in net irradiance of $+2.64\,\mathrm{Wm^{-2}}$ (Fig. 1.1).

Aerosols alter the earth's energy balance by three effects: the direct effect, the indirect effect and the semi-direct effect.

The direct effect is the mechanism, where aerosols scatter and absorb shortwave and longwave radiation. The intensity of this effect depends on the properties of the aerosols, their concentration, and the angle of the radiation to the compounds. While black carbon reduces the albedo and absorbs radiation, sulfate aerosols are highly reflective and have a cooling effect (Wallace and Hobbs, 2006). Scattering of aerosols causes negative radiative forcing, because the radiation is scattered back into the atmosphere. Absorbing aerosols cause warming over bright surfaces, above a white cloud or in a white cloud, because they reduce the albedo. Absorption by aerosols exerts in negative forcing over darker surfaces with a low albedo. The sum of the direct aerosols radiative forcing changes net irradiance by -0.5 $\mathrm{Wm^{-2}}$ (-0.9 to -0.1 $\mathrm{Wm^{-2}}$).

The indirect effect describes the role of the aerosols as cloud condensation nuclei affecting cloud characteristics as radiative property, their lifetime and the precipitation rate. Exhaust fumes may change the optical properties of clouds or increase their area coverage, because the same amount of water concentrates on more potential cloud condensation nuclei. This results in a greater number of cloud droplets with smaller size. Thereby size, chemical composition, mixing state and ambient environment decide about the effectiveness of aerosols acting as cloud con-

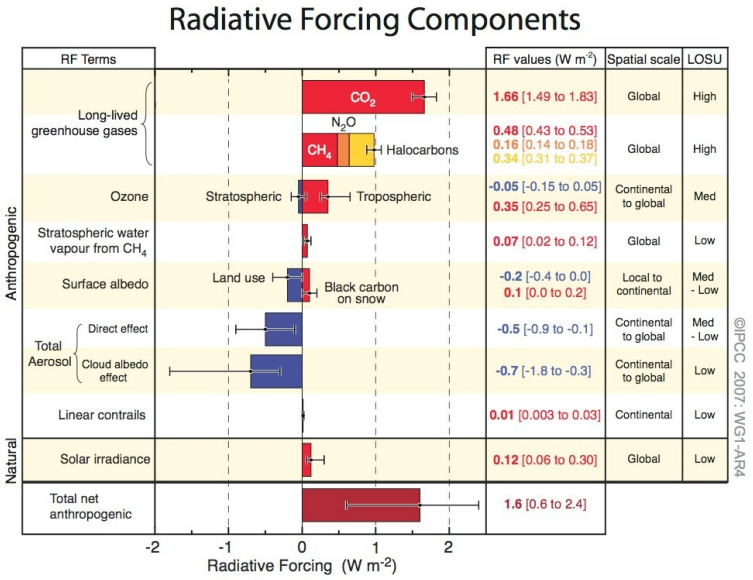

Figure 1.1: The principal components of the radiative forcing of climate change are depicted. The thin black line attached to each colored bar represents the range of uncertainty for the respective value (IPCC, 2007).

densation nuclei (CCN) (IPCC, 2007).

The first indirect effect, or cloud albedo effect includes the change of cloud number concentration and cloud droplet size with fixed liquid water content. The cloud albedo effect causes a negative radiative forcing an reduces the net irradiance at the tropopause by -0.7 (-1.8 to -0.3) Wm^{-2}. The second indirect effect or cloud lifetime effect describes increased cloud lifetime, increased cloud height and drizzle suppression. When the number of aerosols increases, the number of droplets increase while their average size decreases.

The semi-direct mechanism describes the absorption of radiation by aerosols. Absorption of radiation increases the temperature in the environment of the process. Increasing temperature alters the relative humidity and atmospheric stability, e.g. by suppressing convective overturning. This results in evaporation of the cloud. With the evaporation of clouds less solar radiation is scattered back to the atmosphere and thereby the semi-direct effect may have a positive radiative forcing. The semi-direct affect is not considered in the fourth assessment report (AR4) (IPCC, 2007).

1.3 Motivation

The uncertainties of the total aerosol radiative forcing is obviously larger than that of the greenhouse gases, because of the higher variability, shorter lifetime of aerosols and measurement offsets (Hatzianastassiou et al., 2007). Additionally, the scientific understanding is described as medium to low (IPCC, 2007). Increasing the scientific understanding, improving the measurement devices and constraining those uncertainties is an aim of the CLACE (Cloud and Aerosol Characterization Experiment) campaigns.

One major issue of the CLACE2010 campaign was to investigate air mass and clouds dynamics. With the help of the remote sensing instruments wind profiler and ceilometer at the Kleine Scheidegg clouds can be detected and the wind field can be analyzed.

The analysis of the PBL is of interest for verification of greenhouse gas emissions in atmospheric models (Haij et al., 2007). Planetary boundary layer is the lowest part of the troposphere and strongly influenced by the surface (Stull, 1988). Anthropogenic emissions are mainly emitted into the PBL, whose thickness varies from tens of meters to hundreds of meters. The condition of the PBL, its dynamics and mixing processes, influences dispersion of pollutants and hence, the quality of the air we breathe. All atmosphere-surface interactions take place within the planetary boundary layer. These interactions are principally drivers of weather and climate phenomena. Hence, the planetary boundary layer is source of heat, water and turbulence. Therefore, it is important to take the boundary layer and its processes into account for daily weather forecast as well as for climate simulations. Furthermore, dispersion models of pollutants, e.g. after chemical or nuclear accidents, are of interest. To verify models output and to monitor the PBL height, automatical detection by remote sensing instruments and compatible algorithms is aimed.

Long-term series within the global atmosphere watch observes mainly aerosol background concentration at the Jungfraujoch, but injections from the PBL are observed in spring and summer under convective conditions (Collaud-Coen et al., 2011). An important issue is the investigation of the PBL behavior in the complex topography of the Bernese Alps. Therefore, planetary boundary layer height is first derived by ground-based remote sensing instruments, second compared with in-situ measurements at the Jungfraujoch and thirdly compared with the PBL height derived by the COSMO-2 model.

2 Physical basis

2.1 Mountain meteorology

Mountains modify the atmosphere as they are a source or sink of sensible and latent heat flux. They deform main flow and enhance friction and dissipation by mechanical and thermal effects (Barry, 2005; Whiteman, 2000).

Warming effects are modified by slope aspect and inclination and cause thermal differences. Less solar radiation is needed to heat up the same air volume as over lowlands with a ratio of about 2 or 3:1. This fact causes temperature differences between both areas, resulting in density and pressure differences and local wind systems, the along-valley winds (Barry and Chorley, 2003). Across-valley winds are the second feature of the three-dimensional circulation of a valley (Fig. 2.1). The formation of the across-valley winds is driven by horizontal temperature gradients between the surface layer on a slope and the air at the same altitude over the valley center. A pressure gradient develops from the slope to the center, when solar radiation heats the slopes. After sunset radiative cooling sets in and slope wind are formed. However, local winds are only present, when ambient winds are light, otherwise synoptic or meso-scale winds can modify or eliminate local winds (Barry and Chorley, 2003).

After sunrise solar heating generates upslope, or anabatic winds (see Fig. 2.1, panel A) under the stable core, while subsidence prevails above the inversion core. Meanwhile the cold stable core sinks and replaces the warm air, which left the valley. Therefore, the mixing layer (ML) rises much slower than expected due to up-slope mass fluxes. The nocturnal mountain wind, which is still active early in the morning (Fig. 2.1, panel A), ceases (panel B) and reverses to a valley wind (panel C). During day there is a warm valley wind and a cool anti-valley wind aloft and the up-slope wind ceases due to decreasing solar radiation in the afternoon (panel D). In the evening turbulence decays and radiative cooling of the mountain surface causes cold down slopes, the katabatic winds (panel E). The cold air fills pools and the ground of the valley and displaces warmer air upwards (F). As the valley fills with cold air, the katabatic wind ceases. During night time the along-valley wind is a drainage wind down the valley with a corresponding warm anti-mountain wind aloft (panel G-H) (Bendix, 2004; Defant, 1951).

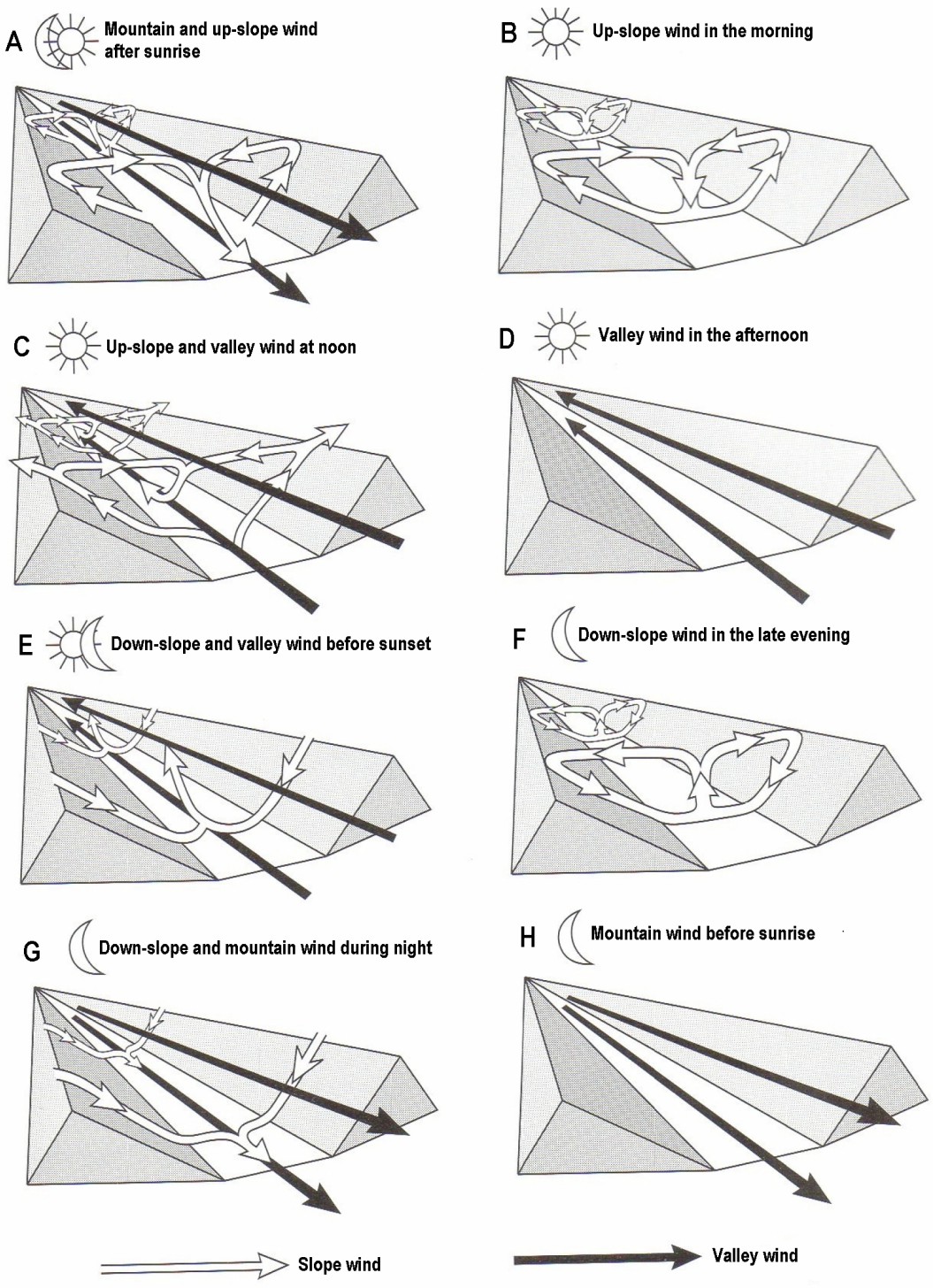

Figure 2.1: Idealized mountain-valley circulation during symmetric cooling and heating of the slopes (Bendix, 2004), modified.

2.2 Planetary boundary layer

The troposphere can be divided into free troposphere (FT) and planetary boundary layer. The PBL is the "part of the troposphere that is directly influenced by the presence of the Earth's surface, and responds to surface forcing within a timescale of about an hour or less" (Stull, 1988). The boundary layer thickness varies from tens to hundreds of meter and during periods with highly instable stratification the PBL height might be up to 4000 m. The planetary boundary layer height usually underlies a diurnal and annual cycle and depends on weather situations, topography and surface roughness (Garratt, 1992).

Whereas mean wind is responsible for horizontal transport or advection, turbulence drives the vertical transport of moisture, heat, momentum and chemicals. Turbulence is one of the main characteristics of the PBL and it is sometimes used to define the PBL (Stull, 1988). Turbulence is mainly thermally induced by buoyancy, secondly mechanically produced by frictional drag, forced convection, wind shear or wake turbulence, and thirdly inertially induced by dissipation of larger eddies to smaller ones (Weigel, 2005). Buoyancy is often organized in thermals and plumes with weak downdrafts in between. Heat transfer from the warm surface creates warm rising thermals. The structure of thermals is smaller at ground level and growths with height to thermals with a diameter up to one kilometer. Thermals often reach the lifting condensation level (LCL) in the afternoon if the air is rich in moisture, leading to cloud formation. Radiative cooling due to clouds creates thermals of cool air sinking from the cloud top (Stull, 1988).

In general the PBL is thinner in high pressure than in low pressure regions and defined by rather cloud free regions (Stull, 1988). Planetary boundary layer air is transported by horizontal divergence to low pressure regions, where PBL air is carried by upward motions, which complicates to define the PBL top.

2.2.1 Diurnal cycle of planetary boundary layer height

Solar radiation is the main driving force for development and diurnal cycle of the PBL. Shortwave radiation is absorbed by the ground, heats up near surface air packets, induces unstable environment and triggers turbulence and latent and sensible heat flux from the ground into the atmosphere.

The planetary boundary layer is divided into different layers with their own characteristic (Fig. 2.2).

The surface layer is the lowest layer next to the surface. During night the PBL consists of a stable boundary layer and a residual layer which is termed while during day a mixing layer prevails from sunrise to sunset. A capping inversion or entrainment zone is the highest layer of

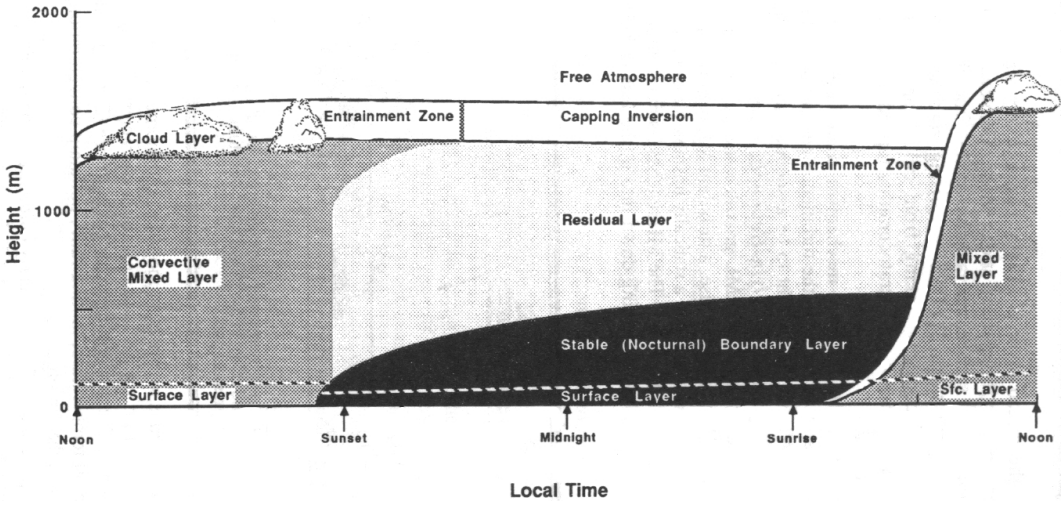

Figure 2.2: Diurnal cycle of a planetary boundary layer in high pressure regions (Stull, 1988).

the PBL over the whole day (see Fig. 2.2).

The surface layer has a vertical extent of typically 10% of the PBL. Turbulent fluxes and stress are almost constant in height. The interstitial layer is located between surface layer and surface, where molecular transport dominates.

Solar heating begins to break up a stable stratified nocturnal boundary layer thirty minutes after sunrise and a shallow mixing layer (ML), also known as convective boundary layer (CBL) deepens slowly. Once the inversion is destroyed, thermal plumes rapidly penetrate through the residual layer, which is the relict of the former mixing layer, to the inversion layer or entrainment zone. The inversion layer is characterized by a temperature inversion between the colder PBL air and warmer air aloft. Thus, it defines the upper extent of the boundary layer, because it suppresses turbulence so that the response to the diurnal temperature cycle is much larger within the PBL (Wallace and Hobbs, 2006).
Reaching the capping inversion, the ML growth slows down and is triggered by entrainment from air of the free troposphere. This entrainment is generated by inertia of thermal plumes, which overshoot the capping inversion before they sink back to the mixing layer. Thereby, a pressure gradient is created causing air parcels from free troposphere to enter the mixing layer. Actually, mixing layer grows by entrainment. Entrainment is also a leading process to dissipate the nocturnal boundary layer (Stull, 1988).

On fair-weather days with sufficient moisture PBL top can exceed the lifting condensation level (LCL) and cumulus clouds are formed. Boundary layer clouds have a suppressing effect on convective activity by downward radiative cooling from the cloud top. In PBL clouds most

of the entrained air comes from cloud base or cloud top, indicating a smaller spread of cloud droplet size distribution. Entrainment of air from the top is caused by turbulent kinetic energy from negatively buoyant downdraft or sinking of other entrained air. Mixing at cloud top is also caused by small updrafts in the middle of a cloud, which becomes wider near the cloud top (Stull, 1988).

Around sunset turbulence weakens and the ML decays. The mixing layer smoothly blends into the residual layer (RL), where heat, moisture and pollutants of the former day persist and turbulence decays. A stable nocturnal layer is formed due to radiative cooling and negative heat fluxes. Within a stable layer a thin low-level jet can be observed with a maximum wind speed of 10-20 m/s usually 100 to 300 m above ground. There are many possible causes for low level jets: baroclinicity, fronts, thermal winds, advective acceleration or mountain-valley winds. Any turbulence is generated by wind shear along the ground level jet, because the statically stable air suppresses turbulence. Despite of the nocturnal jet, wind velocity is usually calm within the nocturnal boundary layer. A stable boundary layer also occurs during daytime caused by warm air advection over a cold surface (Stull, 1988).

As most of atmospheric constituents are emitted near the surface, a large amount of atmospheric aerosol mass is located in the PBL (Jaenicke, 1992). In the convective mixed layer atmospheric compounds disperse vertically by convective plumes, restrained by the capping inversion, which is characterized by a strong gradient of aerosol concentration. In the stable layer constituents disperse rather horizontal, while in the RL constituents tend to disperse in vertical and lateral direction at equal rates.

2.2.2 On the determination of the planetary boundary layer height

The planetary boundary layer height is often determined by the temperature profile, which expresses the stratification of the atmosphere. Virtual potential temperature (Θ_v), which is corrected for moisture and adiabatic pressure changes, is often used to characterize stability (Haij et al., 2007).

$$\Theta_v = T_v(\frac{p_0}{p})^{\frac{R_d}{c_p}} \tag{2.1}$$

Where p_0 is the reference pressure (10^5 Pa) and p the air pressure, R_d is the gas constant of air, c_p the specific heat capacity at constant pressure and $R_d\, c_p^{-1} = 0.286$. $T_v = T(1 + 0.61 q_v - q_l)$ is the virtual temperature, where T represents the air temperature, q_v and q_l are the water vapor specific humidity and liquid water content.

Lapse rate Γ of the virtual potential temperature can be compared with dry or wet adiabatic

situations to derive the local atmospheric stability at a certain height z.

$$\Gamma = \frac{\Delta \Theta_v}{\Delta z} \tag{2.2}$$

The turbulence causes a uniform vertical distribution of heat, moisture and momentum within the PBL. The virtual potential temperature is superadiabatic in the surface layer due to the positive heat flux near the ground. Lapse rate is constant in PBL, close to the dry adiabatic lapse rate, which indicates an absolutely unstable situation and enhances turbulence. The entrainment zone, where air entrains from the FT into the PBL can be classified as a capping stable layer with a temperature inversion. The lapse rate increases with height in the free troposphere, which indicates a stable stratification suppressing vertical displacement of air parcels (Fig. 2.3).

The virtual potential temperature is often used to derive the PBL height, as the average height of the inversion, with the help of radiosonde data (Stull, 1988).

The water vapor content is much higher in the PBL due to evapotranspiration from the surface. Thus, a pronounced decrease is detected across the top of the PBL.

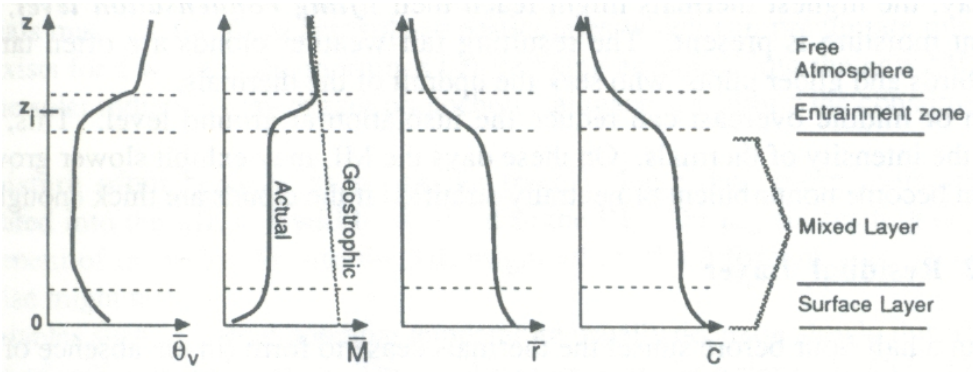

Figure 2.3: Typical daytime profiles of mean virtual potential temperature ($\overline{\Theta}_v$), wind speed $\bar{M}$ ($M^2=u^2+v^2$), water vapor mixing ratio ($\bar{r}$) and pollutant concentration ($\bar{c}$) in the planetary boundary layer. Adapted from Stull (1988).

A further method to estimate the PBL height is to analyze the aerosol concentration. The aerosol concentration builds up within the PBL as most of the aerosol sources are near the Earth's surface and the entrainment zone or capping inversion acts as a lid. In contrast, the aerosol concentration is very low in the FT.

The wind speed within the PBL can be described by a logarithmic wind profile, which is calculated by friction velocity u^* [ms^{-1}] divided by the Karman constant k times natural logarithm of the height z divided by the surface height z_0.

$$\overline{V} = \frac{u^*}{k} \ln \frac{z}{z_0} \tag{2.3}$$

The wind speed increases logarithmically from the surface in dependence of the stability with height, but is constant in the middle layer. While friction is the dominant force near the surface, it becomes less with height, the wind direction turns with height as the geostrophic component increases. Wind direction crosses the isobars with a small angle to low pressure below the PBL top, while the wind changes to geostrophic above the entrainment zone. Hence, wind shear is concentrated in the surface layer and in the entrainment layer and contributes to turbulence generation.

The air temperature decreases due to radiative cooling during night, which can lead to dew or frost formation. As the capping inversion is also present during night, the aerosols remain in the PBL. The stable boundary layer air consumes turbulent kinetic energy, and thus only weak or sporadic turbulence exists.

2.2.3 Planetary boundary layer over mountainous regions

The knowledge of PBL over mountainous terrain is rather incomplete and most studies are based on highly simplified and idealized mountains or undulating areas (Stull, 1988; de Wekker et al., 2004; Weigel, 2005) although mountain areas account for 20% of the land surface (Barry, 2005).

The planetary boundary layer over complex topography is clearly modified by their dynamic influence on the atmospheric characteristics. Planetary boundary layer height increases with increasing altitude of the mountains due to strong warming over daytime. Additionally air masses are forced to ascend on the windward slope of the mountains, transporting also PBL air upward. This is defined as advection venting (Fig. 2.4). Upslope winds can also increase the PBL height (mountain ventilation). When they are very strong they might trigger vertical exchange of PBL air into the FT. On the other hand FT air can enter the PBL by entrainment especially in the luv of the mountain range. Cloud venting defines the process of air exchange between the PBL and free troposphere caused by cumulus formation in combination with strong upslope winds.

Gap flows as foehn are able to deform the PBL into many sublayer and heterogeneous depth (Weigel, 2005). Subsidence occurring during afternoon can lead to a stabilization of the upper boundary layer in a valley.

There is a controversy how PBL follows the terrain (Kossman, 1998; Bendix, 2004), and if aerosol layer and CBL are the same over steep terrain (de Wekker et al., 2004).

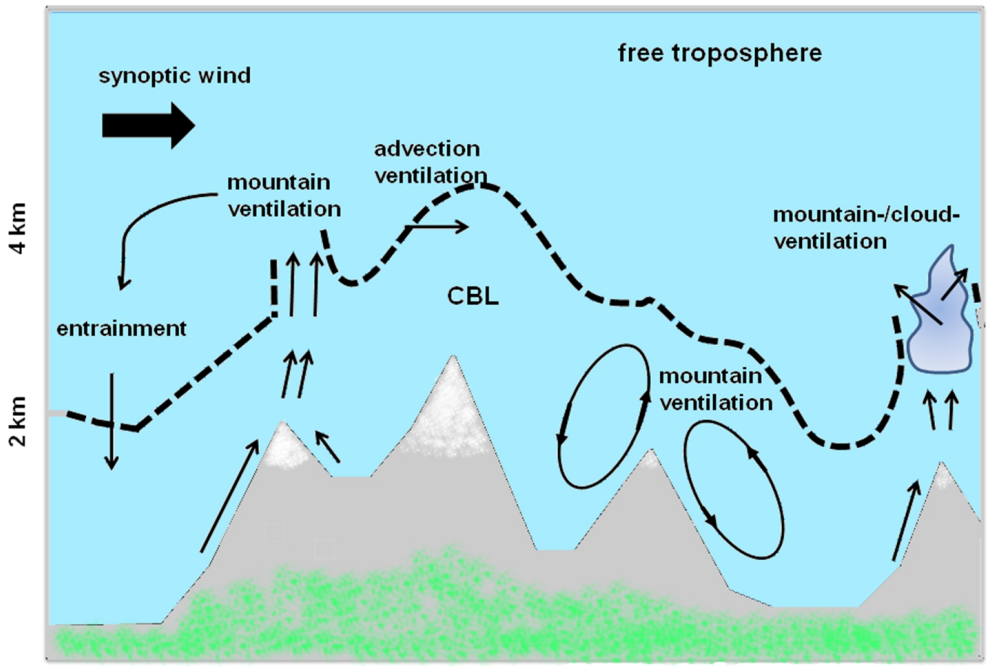

Figure 2.4: Planetary boundary layer over mountainous terrain is modified by slope and valley circulation. Mountain ventilation is caused by strong upslope winds and transports planetary boundary layer air into the free troposphere. Also active cumulus clouds can transport PBL air into the free troposphere. Entrainment can transport air from free troposphere into the planetary boundary layer. Synoptic wind advects layer of planetary boundary layer air over several kilometers (Kossman, 1999, modified).

2.2.4 Planetary boundary layer at the Jungfraujoch

The background concentrations of gas phase species and aerosols in the free troposphere are mainly measured at the JFJ. The measurements are not directly influenced by anthropogenic pollution, except of local pollutions at some specific times. Nevertheless, injections from the PBL reaches the JFJ during thermally-driven convective events (Lugauer et al., 2000) from late spring to late summer (Nyeki et al., 1998), affects spatial and temporal distribution of aerosol properties (Nyeki et al., 2000; Henne et al., 2005). These events occur less often in autumn (Lugauer et al., 2000).

Nyeki et al. (2000) describes that "transport mechanism of air masses to the JFJ depends mainly on CBL growth, rather than on local thermally -induced winds. Although some evidence for these winds are seen [...] on the northern flank of the JFJ massif [...]" Mountain ranges enable handover processes, i.e. exchange of PBL air mass into FT by cloud or mountain venting (Kossman, 1998). The outcomes are elevated aerosol layers, which are transported by advection (Nyeki et al., 2002). A study of Nyeki et al. (2000) with airborne lidar shows a near uniform height of the PBL in the late afternoon at 4200 m a.s.l. over the whole area.

Lugauer et al. (1998) describes the transport of aerosols to the JFJ, which is strongest under anticyclonic high pressure. He divides the PBL into a convective boundary layer above the Swiss Plateau with a maximum height of 2 km (CBL1). By upslope winds CBL1 is transported to high-alpine sites (CBL2). On its way, PBL air mixes with FT air. Therefore, alpine PBL air is diluted in contrast with the PBL air over the Swiss Plateau. The aerosol concentration increases at the Jungfraujoch during afternoon until 18:00. Horizontal winds remove the air masses with elevated aerosol concentration at the Jungfraujoch during night.

To classify the aerosol measurement at JFJ, it is important to know, which air masses influence the ambient concentrations (Nyeki et al., 1998).

2.3 Planetary boundary layer height detection

The planetary boundary layer height can be detected by several instruments and methods. The instruments can be divided in direct measuring techniques and aircraft based or ground based remote sensing measurements.

Radiosondes, tethered balloons or in-situ measurements are among the first group. Radiosondes provide vertical temperature, humidity and wind profiles on certain times of the atmosphere. They are a common source for operational planetary boundary layer height determination, because they are in use all over the world, launched twice or maximal four times daily and the instruments and data are quality controlled. Comparisons between conditions in the PBL and the free troposphere or with PBL height derived by numerical models can be made. Smoothing due to the high ascent rate is one reason for high uncertainties of the PBL height. Another disadvantage is, that continuous monitoring of the PBL height is not possible, because straightforward interpretation of temperature, humidity, wind and turbulence profiles is not possible for the nocturnal PBL (Seibert et al., 2000).

The Bulk-Richardson method is a commonly used method to estimate the PBL height. Bulk-Richardson number Ri_{B} represents the ratio of thermally produced turbulence and turbulence generated by wind shear. Planetary boundary layer height is determined, when the Bulk-Richardson number exceeds a certain threshold, e.g. 0.21 is widely used in literature. Bulk-Richardson number is calculated by gravity g divided by virtual potential temperature (Θ_v) and vertical differences of Θ_v and the horizontal fluxes (U and V) (Stull, 1988)

$$Ri_B = \frac{g}{\bar{\Theta_v}} \frac{\Delta\bar{\Theta}_v \Delta z}{[(\Delta\bar{U})^2 + (\Delta\bar{V})^2]} \tag{3.1}$$

Another method for planetary boundary layer height estimation is the parcel method. This method determines "the height of the intersection of the actual potential temperature with the dry-adiabatic ascent" (Hennemuth and Lammert, 2006) from the temperature at the lowest

reported level.

Tethered balloons can be equipped with numerous measurement devices to measure turbulence or trace gases, but they are mostly linked to field campaigns and a certain measurement range below 1000 m.

In-situ profile measurements of temperature, humidity and wind along a mast or tower have a high resolution and operate continuously, but the limited range and high costs are the shortcomings (Seibert et al., 2000). However, it is one opportunity to measure turbulence (Beyrich et al., 2010). Masts with heights of 10 to 50 m are primarily useful to do surface measurements, while towers with heights uo to 444 m are useful to study shallow nighttime and early morning boundary layer heights (Stull, 1988).

Remote sensing measurements, which suit for PBL height estimation, are acoustic instruments (sodar), electro-magnetic (wind/radar profiler) and optical instruments (lidar, ceilometer). Sodar (sound detection and ranging) emits sound waves and measures the scattering of sound waves by temperature in homogeneities, determined by the acoustic refractive index C_n^2. Profiles of mean wind and vertical velocity variance can be determined and used for PBL height estimations. Important advantages of sodars are the suitability for stable and convective boundary layer and the low height of the first measurement of 40 m over the instrument, which makes the sodar suitable for nocturnal PBL detection. However, the vertical range of the sodar is also limited to 1000 m above the instrument, and consequently, no deep boundary layers can be detected. Wind profiler, lidar and ceilometer are already described in chapter 2.5 on page 17. The combination of acoustic with optical or electromagnetic remote sensing may lead to the best and most complete information of the PBL (Emeis et al., 2006).

2.4 CLACE campaign

The CLACE2010 campaign took place at the Jungfraujoch (46°32'N, 7°59'E, 3580 m a.s.l.) and at the Kleine Scheidegg (2061 m a.s.l.) in the Bernese Alps from June to August 2010. The international foundation high altitude research stations JFJ and Gornergrat, which are accessible by train, provide the infrastructure for scientific work and also for CLACE campaigns. Several CLACE campaigns have been carried out by international and institutional collaboration at the JFJ during the last years in summer and winter. Goals of the campaigns are to study chemical and physical characteristics of aerosols, to investigate the direct and the indirect aerosol effect. For example, the interaction of aerosol particles with clouds through droplet and ice crystal formation, the aerosol optical and hygroscopic properties or new particle formation are investigated at the JFJ. Furthermore, over 17 years of continuous aerosol measurements are performed by the PSI at the JFJ within the global atmosphere watch (GAW) program of the World Meteorological Organization. Additionally, a SwissMetNet Station is operated at the JFJ.

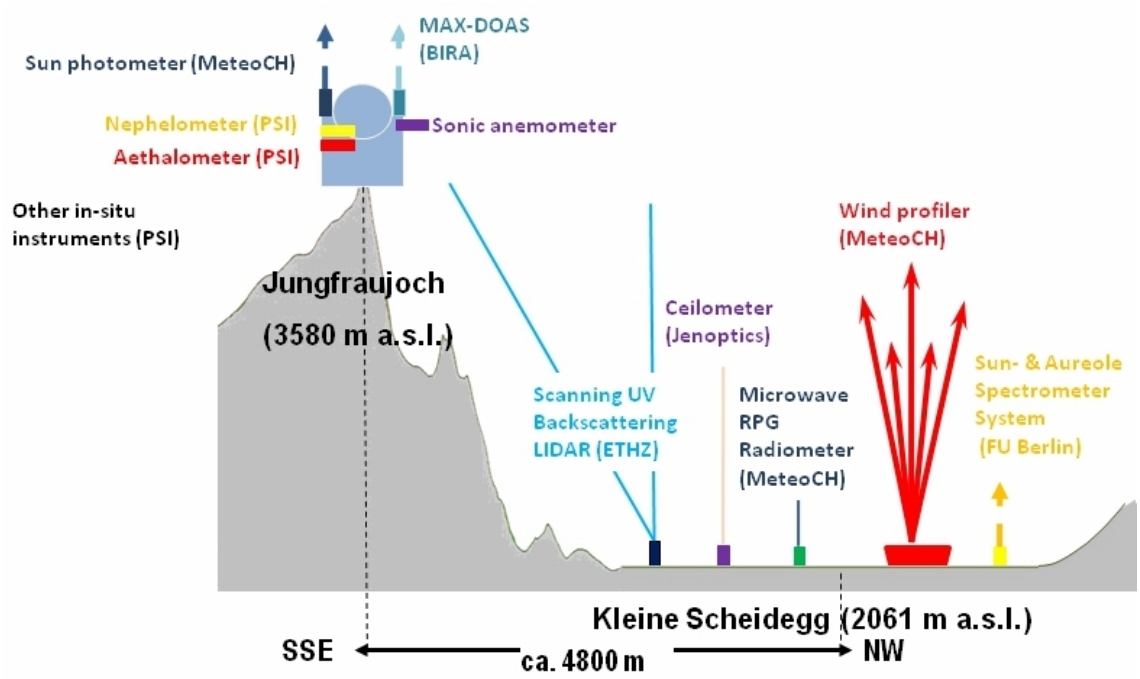

Figure 2.5: Set-up of the CLACE2010 campaign at the Jungfraujoch and Kleine Scheidegg.

The main goals of CLACE2010 were an in-depth characterization of the cloud microphysical processes at the Jungfraujoch, extending the knowledge gained during earlier CLACE campaigns, investigation of the planetary boundary layer and an optical closure study.

Amongst others, nephelometer, aethalometer, cloud condensation nuclei counter (CCNC), HS ultrasonic anemometer (Gill Ltd., Solent, U.K.) and fog monitor were installed (Fig. 2.5.

The optical properties of the aerosol layer at and around the Jungfraujoch were examined using a variety of remote sensing equipment. The remote sensing experiments were also performed at the Kleine Scheidegg for the first time. A wind profiler LAP-3000 (Vaisala, 2007b), a microwave radiometer, a ceilometer CHM15k (Jenoptik, 2009), a sun- and aureole spectrometer, polarimeter and scanning UV backscatter lidar were located at the Kleine Scheidegg (see Fig. 2.5).

The Jungfraujoch is a saddle between the Jungfrau (4158 m a.s.l.) and the Mönch (4107 m a.s.l.) in southwestern and northeastern direction. The Great Aletsch Glacier is located southeast of the JFJ and the Kleine Scheidegg is located northwestern direction. The Kleine Scheidegg is located between the Lauberhorn (2472 m a.s.l.) and Eiger (3970 m a.s.l.) and connects Grindelwald with Lauterbrunnen (see Fig. 2.6).
Figure 2.6 depicts the topography of the measurement sites and shows also wind roses at the Kleine Scheidegg and at the Jungfraujoch. At the Jungfraujoch mainly NW winds and secondary SE winds are measured. Whereas at the Kleine Scheidegg mainly SW winds and secondary SE

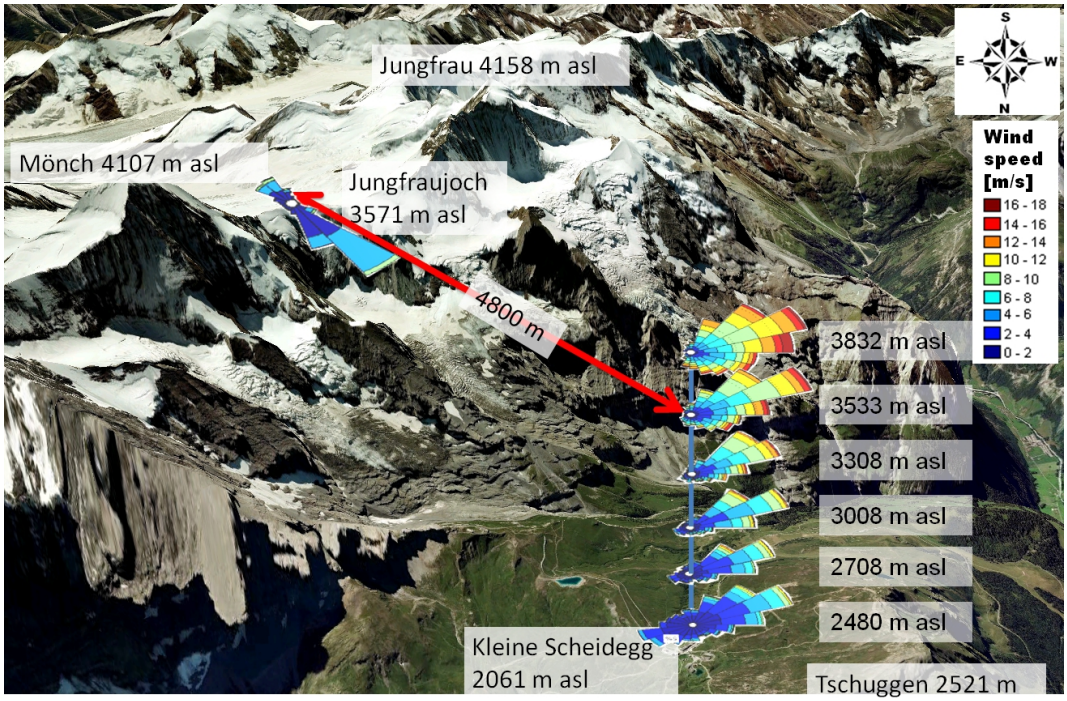

Figure 2.6: Satellite image of the region Eiger, Mönch and Jungfrau. Wind rose at the Kleine Scheidegg is plotted using wind profiler high mode data at the height of 2409 ± 102 m for KLS. At the JFJ the data for the wind rose is from the Rosemount anemometer, which is installed at the top of the 10 m mast on the tourism platform (Background: Google Earth).

winds are observed by the wind profiler, because the wind fields at both measurement sites are strongly influenced by the topography (further explanations, see chapter 4.1).

2.5 Remote sensing instruments

2.5.1 Wind profiler

A wind profilers emit and receive electromagnetic radiation which is partly scattered by targets. Small amounts of backscatter return and can be measured by the wind profiler with a definite time delay, which is used to calculate the height of the target. Backscatter is sampled during sequential intervals, referred to as range gates. Consequently, the backscatter is related to discrete altitudes. Targets, which cause backscatter, are refractive irregularities (Cost Action 76, 2001). Refractive irregularities are a function of the density of the atmosphere. They are caused by variations of temperature, humidity and pressure over short distances, which are generated by turbulence. Refractive irregularities change the characteristic of the electromagnetic energy on their way through the atmosphere. Refractive irregularities carried by the mean wind, are detected by the wind profiler and give us information about the wind itself. Maximum backscattering occurs when the irregularities are about half of the size of the radar wavelength. This phenomenon, called Bragg scattering, often appears at air mass boundaries with associated turbulence and strong gradients of refractive index along these boundaries, as well as cloud and fog tops or stable layers (James, 1980).

The return signal is analyzed in real time by the system in two steps: the time-domain and frequency-domain stage. In the time-domain stage the samples are coherent averaged and the DC voltage is removed. The fast fourier transformation (FFT) converts the sample to the frequency domain stage, followed by windowing to reduce mathematic artifacts of the FFT and spectral averaging (Vaisala, 2007a). The quantities noise level, signal power, spectral width and Doppler shift are calculated from the frequency spectrum obtained for each range gate, centered at the middle of the measured layer (Vaisala, 2007a; Ruffieux and Stübi, 2001).

Horizontal wind speed and direction are determined by combining the Doppler shifts of all beams. The Doppler principle describes a wave, which shifts in frequency due to the motion relative to the observer. These frequency shifts are proportional to the wind speed (Emeis et al., 2006), which can be calculated on this way. The vertical beam measures vertical wind velocity.

Available parameters provided by the wind profiler software for each beam and each mode are Doppler shift, spectral width, noise level and signal-to-noise ratio (SNR). Spectral width is the second moment or spread of the spectrum. Signal-to-noise ratio is a measure of the wind profiler performance. Low SNR shows a degraded performance of the wind profiler caused by high background noise, neutral lapse rate and less turbulence and dry conditions.

An important assumption is a homogeneous wind field over the beams' separation. However, homogeneity can not be guaranteed in the complex topography of the Bernese Alps.

Wind profilers very weak clear air signal can easily be contaminated. Erroneous data are cre-

Figure 2.7: Picture of the Vaisala wind profiler LAP-3000 at the Kleine Scheidegg.

ated due to low SNR in stable air with laminar flow, birds and insects crossing the beam or moving cars and trees affecting the side lobes of the antenna (Wilczak et al., 1995). Wind profilers measure rather the movement of the hydrometers during precipitation. Incorrect data are produced by topographical induced turbulence or highly convective conditions (Vaisala, 2007b).

The Vaisala wind profiler LAP-3000 (Vaisala, 2007b) was located at the Kleine Scheidegg (Fig. 2.7). The wind profiler LAP-3000 has five beams with one vertical and four oblique beams tilted by 15 ° in the four orthogonal directions. The wind profiler works with 1290 MHz frequency and a wavelength of 23.2 cm (Tab. 2.1). The duration of the transmitted pulse determines the depth of a layer and thus the spatial resolution, also called range gate.
The wind profiler runs in two modes: low mode and high mode.

Operating frequency	1290 MHz
Peak power	600 W
Direction	zenith and ±15.5° in 4 orthog. directions
Beam width	∼ 9 °
Minimum measurement height	120 m
Maximum measurement height	2-5 km
Range gates	72 m, 204 m

Table 2.1: Technical specifications for the wind profiler LAP-3000.

The resolution of the high mode is coarser (204 m) but the larger the vertical resolution the more energy is scattered back and received by the wind profiler and the better signal (Tab. 2.1). In the low mode the vertical resolution is better (72 m), but the SNR is weaker due to the

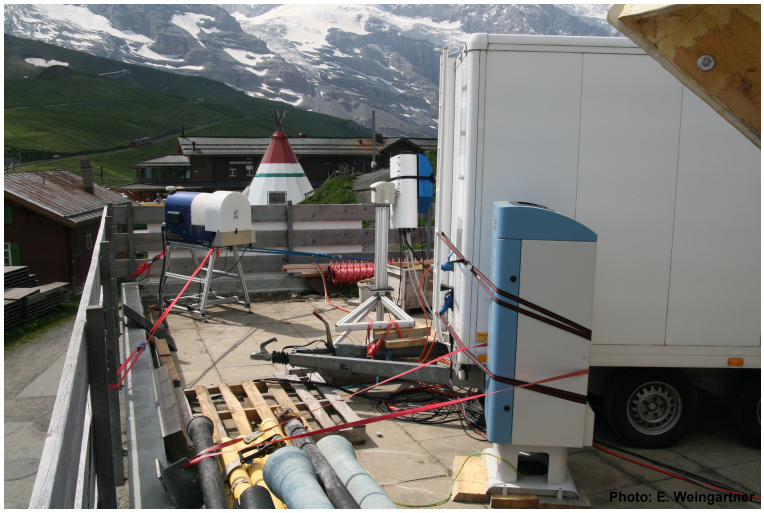

Figure 2.8: Picture of the Jenoptik ceilometer attached to the monitoring trailer at the Kleine Scheidegg. Lidar and microwave radiometer are behind this trailer (picture: E. Weingartner).

smaller vertical resolution and therefore less energy is scattered back per range gate (Vaisala, 2007b). The height of the measurements goes up to 5000 m height above instrument depending on the characteristics of the atmosphere. The minimal measurement height during CLACE2010 is 2409 m a.s.l., which means 348 m above the instrument. This is caused by wrong instrument settings, which are not comprehensible.

The wind profiler did not include a radio acoustic sounding system (RASS), which could provide temperature profiles.

2.5.2 Ceilometer

A lidar (light detection and ranging) emits short laser pulses with lengths of few to several hundred nanoseconds into the atmosphere, where they are scattered by air molecules (Rayleigh scattering) and particles (Mie scattering) (Weitkamp, 2005). A portion of the emitted light is scattered back to the instrument. The height of the backscatter can be calculated using the time delay of the signal. Measured backscatter depends on amount and nature of scattering particles and the time interval between transmission and reception of signal determines the correspondent altitude. However, the emitted light can be completely attenuated due to the presence of optically thick cloud, fog and precipitation.

Ceilometers like Jenoptik ceilometer CHM15k are commercial lidars (Fig. 2.2). The Jenoptik ceilometer CHM15k (Jenoptik, 2009) was situated at the Kleine Scheidegg. Separated lens telescopes of 100 mm diameter are used as transmitter and receiver. The ceilometer has a solid state

Wavelength	1064 nm
Spatial resolution	15 m
Temporal resolution	15 sec
Pulse repeat width	5-7 kHz
Measurement height	≈ 200-15000 m

Table 2.2: Technical specifications of the Jenoptik ceilometer CHM15k (Jenoptik, 2009).

Nd:YAG laser at 1064 nm wavelength. The pulse duration of 1 ns defines the vertical resolution of 15 m. Signal detection in photon counting mode is made with an avalanche photodiode. The Jenoptik instrument is able to detect aerosols and clouds from 30 m a.s.l. up to 15000 m above the instrument in cloud free periods.

The sensitivity of the ceilometer on molecular or particles backscattering depends on the wavelength of the laser. Backscattering in the molecular range is almost negligible at 1064 nm. Strong backscattering is caused by high aerosol concentration (clouds or Sahara Dust) using a laser with a wavelength of 1064 nm (Flentje et al., 2009). Below a radius of 1 µm the scattering efficiency decreases significantly (Flentje et al., 2010a). The Jenoptik ceilometer is able to detect lower cloud layers as well as cirrus clouds reliably. Transitions of a aerosol concentrations give the opportunity to detect boundaries in the atmosphere, because the vertical distribution of particles is heavily influenced by the thermal structure of the atmosphere.

The backscatter signal intensity $P(r)$ of a near infrared lidar is a function of the instrument function $C(r)$, the backscatter coefficient β and background signal P_0. This is also known as the lidar equation.

$$P(r) = \frac{C(r)}{r^2}\beta(r)T(r) + P_0 \tag{5.1}$$

where r is the distance and $T(r) = exp(-2\int_0^r \alpha(r)dr)$ is the round-trip transmission factor. All parameters are wavelength dependent, except of distance r. Extinction α and volume backscattering β coefficients are a combination of aerosol and molecular components (Weitkamp, 2005).

Both are the product of particle number density N and scatter cross section σ, which is a function of particle size distribution and the refractive index. Changes in relative humidity influence the amplitude of the gradient due to hygroscopic growth of the aerosols. The instrument function $C(r, \lambda)$ takes precipitation, which interferes the measurements and the overlap correction into account. The minimal measurement height is 200 m, below this height, there is an uncorrectable overlap between the laser beam and the receiver field of view. In this overlap region the small distance between transmitter and receiver, together with a narrow beam result in an incompletely detection of backscatter (Weitkamp, 2005).

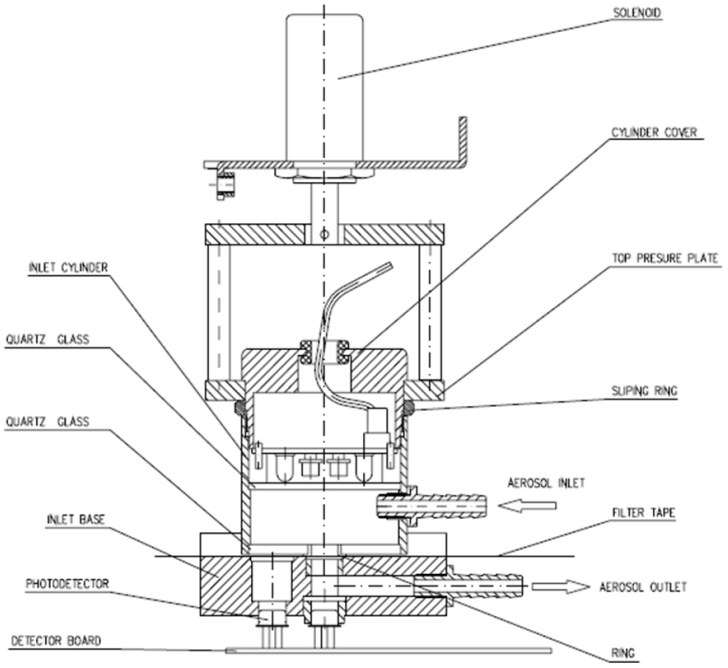

Figure 2.9: Schematic cross section of aethalometer's optical analysis head (Hansen, 2005).

The overlap function is required to expand the processability of ceilometer data downwards from 1500 m to 200 m above the instrument. Geometric overlap of the receivers and transmitter optical field impact the data quality in the lower ranges (Frey et al., 2010). Additionally the lidar equation is linearized to avoid negative values, which allows to calculate noise. The signal-to-noise ratio is defined as "the ratio of incoming signal to the amount of interfering noise" (Heese et al., 2010).

2.6 In-situ instruments at the Jungfraujoch

2.6.1 Aethalometer

Aethalometers are most frequently used filter-based commercial instruments to measure mainly black carbon (BC) mass concentration. Black carbon is defined as the fraction of carbonaceous aerosol absorbing light over a broad band in the visible spectrum. This aerosol fraction is emitted by combustion of any carbonaceous fuel and during biomass burning. The amount of emission depends on combustion process. There are no significant natural sources, despite of volcanoes, which emit relatively small amount of BC, or forest fires (Wallace and Hobbs, 2006). Therefore, the presence of BC at the JFJ is an indicator of combustion processes, most notably from diesel exhaust, which took place e.g. at the Swiss plateau and is transported towards the Jungfraujoch. Additionally, Sahara Dust contributes to small amounts to aerosol absorption at the JFJ (Nyeki et al., 1998), especially at smaller wavelength (Fierz-Schmidhauser et al., 2010).

The aethalometer (AE-31, Magee Scientific) (Fig. 2.9) measures the light attenuation by suspended aerosol particles at the wavelengths $\lambda = 370, 470, 520, 590, 660, 880, 950$ nm. Under the assumption of a certain mass absorption coefficient the black carbon concentration is calculated.

An internal pump draws air through the inlet port and it continuously monitors the flow rate. While the aethalometer collects a sample on a quartz fiber tape, it performs a continuous optical analysis, with a time resolution between two minutes to one hour. The optical attenuation (ATN) is measured, which is defined as the logarithmic relationship between the incoming light (I_0) and the remaining light (I) intensity after passing the filter (Hansen, 2005).

$$ATN = 100 * \ln(\frac{I_0}{I}) \tag{6.1}$$

Additionally, the light intensity after passing a second particle free reference filter is measured to stability of the optical source.

According to Beer Lambert's law, which defines the exponential attenuation of radiation (I_0) by absorption (b_{abs}) and scattering processes in a medium with a certain thickness (x)

$$I = I_0 e^{-b_{\text{abs}} x} \tag{6.2}$$

the aerosol absorption coefficient (b_{ATN}) is calculated.

Light attenuation can be converted to absorption coefficient (σ_{abs}) by (Weingartner et al., 2003)

$$\sigma_{abs} = \frac{A}{Q} \frac{\Delta ATN}{\Delta t} \frac{1}{C * R(ATN)} \tag{6.3}$$

where A is the filtered spot area, Q the volumetric flow rate, ΔATN is the change in attenuation during time interval (Δt). C and $R(ATN)$ are calibration factors. The derived absorption coefficients (σ_{ap}) from aethalometer measurements are, according to Collaud-Coen et al. (2010), systematically to high. To correct multiple scattering C is used as an independent empirical constant, which takes into account multiple reflections of the light beam at the filter fibers. This leads to enhanced light absorption of the deposited particles (Weingartner et al., 2003). Calibration factor C has a value of 2.81 at the Jungfraujoch (Collaud-Coen et al., 2010). Filter loading correction R depends on the amount of aerosols and their optical properties. For unloaded filter R=1 is used and the value decreases the more absorbing particles are deposited, reducing the optical path (Weingartner et al., 2003).

If the particles on the filter consists of only black material, the values are identical at each wavelength (Hansen, 2005). Other materials like mineral dust, inorganic compounds or aromatic compounds may increase the response of the 660 nm, 880-950 nm on 450 nm, due to their coloration or kind of absorption (Hansen, 2005).

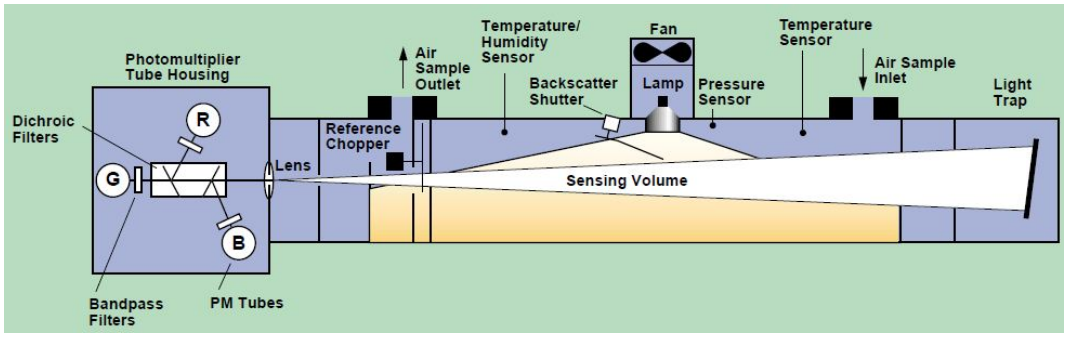

Figure 2.10: Schematic view of the TSI three wavelength nephelometer (picture taken from www.tsi.com).

2.6.2 Nephelometer

An integrating nephelometer (TSI Inc., model 3563) measured the dry scattering coefficient σ_{sp} and dry backscattering coefficient σ_{bsp} of the total suspended particulate matter (Fig. 2.10). Measurement of total (7 ° to 170 °) and backscatter (90 ° to 170 °) signals using a rotating backscatter shutter to block the illuminated sample volume from 7 ° to 90 °. TSI 3563 measures wavelength depending by splitting the light into green ($\lambda = 550$ nm), blue ($\lambda = 450$ nm) and red ($\lambda = 700$ nm) using high-pass and band-pass color filters in front of the photonmultiplier tube detectors. The instrument includes an internal pressure and temperature sensor and is sensitive to light-scattering coefficients as low as $2.0 \cdot 10^{-7}$ m^{-1}.

2.6.3 Condensation particle counter

A condensation particle counter (CPC) detects airborne particles from a diameter of 10 nm upwards. A laminar flow with an aerosol flow rate of 1 l min^{-1} is drawn through a heated supersaturator, in which butanol is vaporized (Fig. 2.11). Afterwards the flow enters a cooled condenser, where condensation takes place, because butanol vapor becomes supersaturated and the particles act as condensation nuclei. Droplets pass through an optical detector, which counts each particle.

The TSI CPC 3772 is used for low aerosol concentrations from 0 to 10^4 particles per cm^{-3}.

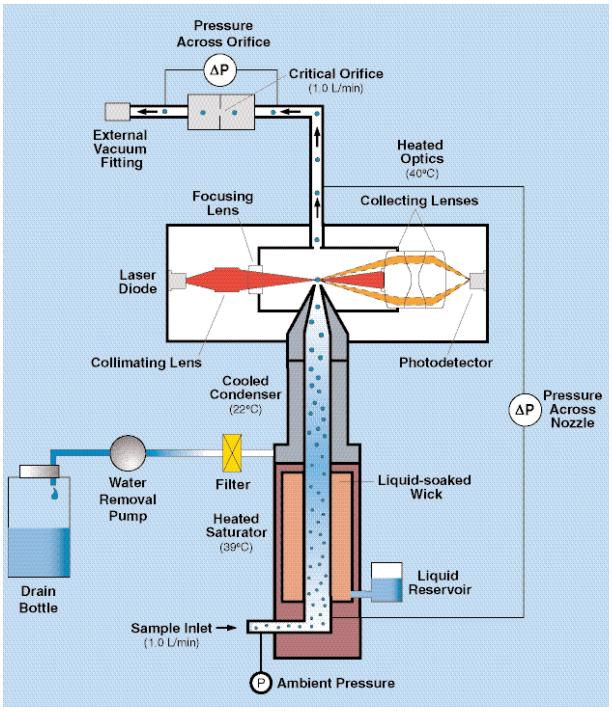

Figure 2.11: Schematic view of the condensation particle counter (picture taken from www.tsi.com).

3 Methods

3.1 Planetary boundary layer height determination using a ceilometer

Due to the fact that sources of aerosols are near the Earth's surface, aerosol concentration is very high in the PBL and thus the signal received by the ceilometer within the PBL is relatively high. The capping inversion layer acts as a lid and aerosols are often washed out in the PBL. Therefore, free troposphere returns a low signal. Additionally the swelling of aerosols due to enhanced humidity at the PBL top leads to a further increases of the signal.

Current algorithms for PBL detection are mainly based on vertical methods. The vertical methods are based on the strongest gradient, which is identified by using the first or second derivative of the range corrected signal, or the first derivative of the logarithm of Pr^2. Wavelet covariance method is another vertical method, where the maximum correlation coefficient between the signal and a wavelet method is used as top of the planetary boundary layer.

3.1.1 Planetary boundary layer height estimation using Jenoptik retrieval

Jenoptik starts for the mixing layer height estimation with Gabor transformation on individual backscatter profiles to decontaminate them and to filter non aerosol backscatter, e.g. returns from clouds, out.

Afterwards the data is smoothed to remove artifacts. Continuous wavelet transformation with Haar-wavelet calculates a spectrogram with a step width of two and for scales 10 to 30. Haar-wavelet is assumed to be a good approximation of multi-scale gradient analysis. To evaluate the wavelet transformed data the wavelet spectrum is applied. Thereby, the wavelet transformed data are integrated. Maxima in the wavelet spectrum indicate the location of the maximal negative change in the range-corrected signal. Thus, maxima in the wavelet spectrum identify boundaries of aerosol layer height (Teschke and Poenitz, 2010; Frey et al., 2010).

With the help of threshold in SNR, the number of neighbors, definition of a maximal PBL height of the lowest layer and a layer above is selected.

In figure 3.1 two Pr^2 profiles are depicted with the corresponding planetary boundary layer height and the threshold of SNR. The first profile (Fig. 3.1, panel A) shows a profile on the fair

weather day 7 July at 12 pm. The strong backscatter signal within the PBL is distinctive from 2200 m a.s.l. to about 2800 m a.s.l.. During night at 22 pm, the backscatter signal decreases with height above 2250 m a.s.l. with two stronger gradients, which are marked as residual layers.

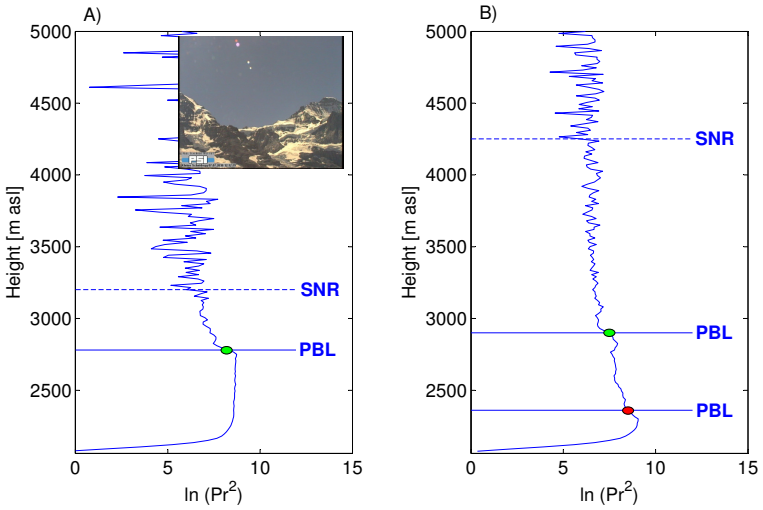

Figure 3.1: Ceilometer Pr^2 profile, planetary boundary layer height (Jenoptik algorithm) and height of SNR threshold ≤1 on 7 July 2010 at 12 pm (panel A) with the corresponding web cam picture from the Kleine Scheidegg towards the Jungfraujoch. During night two residual layers are estimated (panel B). The dots depict the quality of the PBL height estimation according to Tab. 3.1. Green color marks good quality due to a large magnitude of jump in backscatter signal around the PBL height, whereas the red point depicts a weak quality according to a difference of the backscatter signal.

To improve the results, a quality index of (Haij et al., 2007) is applied.

3.1.2 Quality index

A quality index is used to classify the PBL height estimations. The quality index depends on the magnitude of the jump in backscatter ($\ln(Pr^2)$) (Haij et al., 2007). Therefore, the backscatter is averaged in the region of 15 m to 150 m above the PBL height (B_u) and 15 to 150 m below the PBL height (B_d). If less range gates are available, less range gates are taken. The difference between the region above and below the PBL height is divided into three classes (Tab. 3.1).

color	trigger mechanism	description
	B_d-B_u<0.25	poor PBL height detection
	0.25≤B_d-B_u<0.5	weak PBL height detection
	B_d-B_u≥0.5	good PBL height detection

Table 3.1: Classification of the used quality index for planetary boundary layer height detection.

One example of range corrected backscatter signal of the ceilometer with indexed PBL height

determined using the Jenoptik algorithm is depicted in Fig. 3.2.

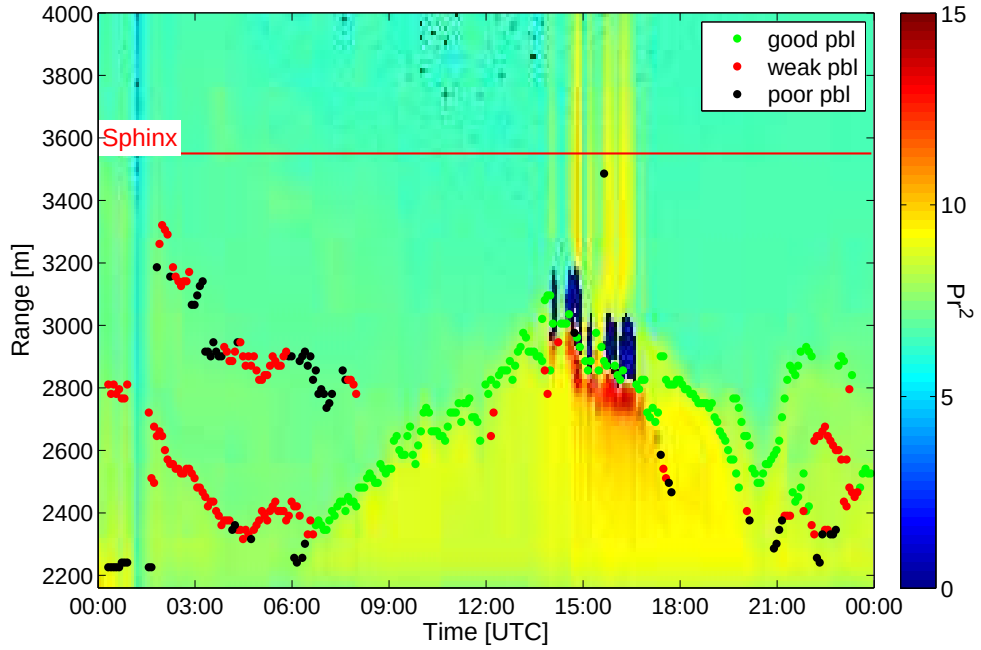

Figure 3.2: Range-corrected backscatter signal (Pr^2) and height of the planetary boundary layer is shown on 7 July 2010. The quality index, which takes the strength of the gradient into account, is used to estimate the quality of the detected PBL height. Good PBL height detection is marked in green, weak PBL height detection is marked in red and poor PBL estimations are colored in black. The red line marks the height of the Sphinx observatory at the Jungfraujoch.

3.1.3 Planetary boundary layer detection using STRAT-2D

STRAT-2D (Morille et al., 2007) uses a combination of wavelet transform and Pr^2 thresholding to estimate the mixing layer height.

Cloud and aerosol layer are detected using wavelet transformation and by comparison of the wavelet transformation coefficients with threshold, defined by the Gaussian distribution.

The continuous wavelet transformation (CWT) is used to identify base, top and peak backscattering of individual particle layers. Then, similarities are searched between Pr^2 and a Mexican hat wavelet ($\Psi(r)$) for each range and scale. Continuous wavelet transformation coefficients can be interpreted as a correlation coefficient between wavelet and Pr^2 are calculated. By means of the modulus of the CWT coefficients the highest anti-correlations and correlations can be identified. The averages CWT coefficients along the ridges give a hint if it is a layer peak or base or top. Afterwards, the difference between peak height and base height is compared with a threshold to remove noisy variations. The threshold is defined on the basis of Gaussian distribution.

The wavelet of the first derivative of Gaussian $\Psi'(r)$ has a similar shape to the negative backscatter signal at the top of the boundary layer height. Subsequently, the gradients of the backscatter signal are detected and the negative gradients are separated using the CWT' coefficients. This is also supported by the wavelet shape. To define the MLH, a combined analysis of the negative gradient, the lowest molecular range and the base line of the lowest particle layer is made (Fig. 3.3) (Morille et al., 2007).

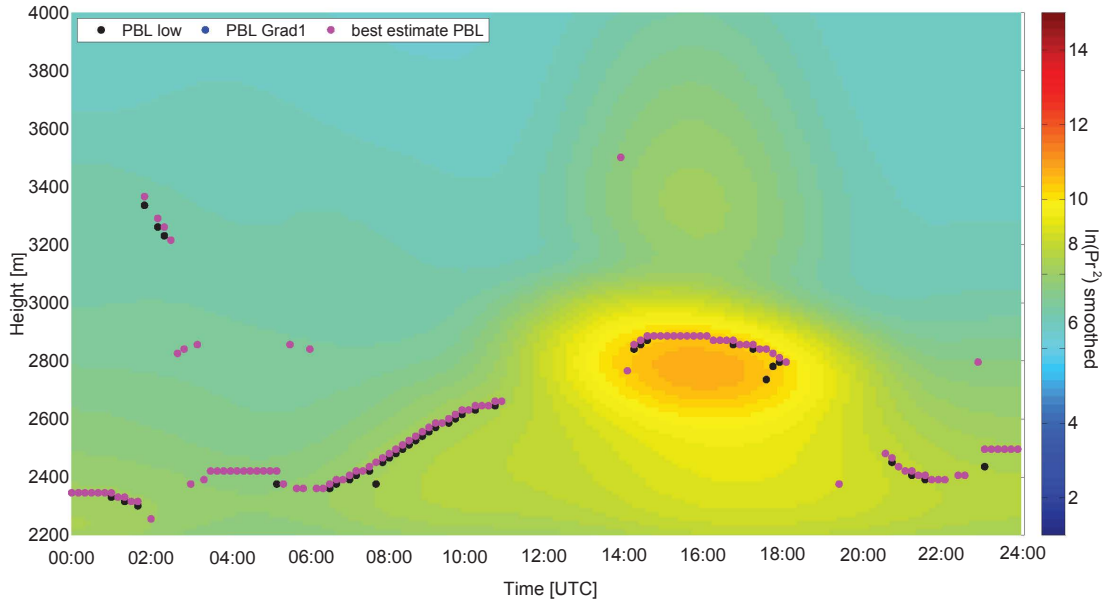

Figure 3.3: Smoothed range-corrected backscatter signal and STRAT-2D PBL estimations (dots) on 7 July 2010.

Disadvantages of the PBL estimation are a missing physical definition of the planetary boundary layer and the absent quality control or evaluation of the PBL. Planetary boundary layer height detection faces two major problems. First, backscatter profiles do not only contain aerosol backscatter and secondly, the gradients occur at different scales, locations and with different sizes (Teschke and Poenitz, 2010). The determination of which edge corresponds to the top of the mixing layer, the lowest gradient or the strongest, is one major difficulty (Haeffelin et al., 2009).

3.2 Planetary boundary layer detection over daytime using a wind profiler

A large humidity gradient near the top of the daytime planetary boundary layer, or convective boundary layer (CBL), large vertical velocity and strong turbulence within the CBL allow the wind profiler to detect the CBL.

Turbulence causes variations of temperature, humidity and pressure, which leads to variation in the refractive index. Variations in the refractive index are measured by the refractive structure parameter, which is proportional to SNR of wind profilers backscatter power. Consequently, range-corrected SNR can be an effective method to analyze the CBL. However, cloudy sky, precipitation, aloft subsidence inversions hampers PBL detection. Furthermore, PBL is ineffective to be detected during night (Vaisala, 2007b). Additionally, wind profilers have a too high lowest range gate to detect shallow boundary layers.

The wind profiler data show unusual fluctuations throughout all measured parameters during the first 10 days of measurement as a result of wrong instrument settings, which are not traceable. Also wrong wind directions were measured during the period from 29 June to 09 July 2010 at 8 pm. Therefore, wind direction was corrected by 180° and u and v are multiplied by -1.

Two datasets of wind profiler data exist: 30 minutes averaged data, processed by the Vaisala Program, which makes also a first quality control. The second dataset consists of radial velocity, SNR and spectral width for every beam for low and height mode in a temporal resolution of about 6.30 min. Data with a signal to noise lower than -15 dB are not considered (Gaffard et al., 2001).

Signal-to-noise ratio is equal to 10 multiplied by the logarithm of total signal power divided by noise power.

$$SNR[dB] = 10 * \log \frac{\text{total signal power}}{\text{noise power}} = 10 * \log \frac{\text{total signal power}}{\text{noise density} * \text{number of points}} \tag{2.1}$$

Signal-to-noise ratio and noise density are two parameters, which are calculated and can be archived by Vaisala software LAP-XM.

The Vaisala software does not provide range-corrected SNR value as an output although it is used internally in the following firmware: the consensus, melting layer module, the consensus module optional NOAA precipitation correction algorithm and melting layer module. But the range-corrected SNR are not accessible outside the algorithm. Thereby the range correction SNR is calculated as follows:

$$SNR_{corrected}[dB] = SNR + 20 * \log(\text{measurement height [m]}) \tag{2.2}$$

LAPMom does graph range corrected SNR values, but they are calculated within the applications. The correction factor used is:

$$SNR_{corrected} = (SNR) + (20 * \log \frac{\text{measurement height [m]}}{\text{first range gate height[m]}} \tag{2.3}$$

A calibrated value of a range corrected SNR can be calculated in the form

$$dBZ[dB] = (SNR) + 20 * \log(\text{measurement height}) - (A) \tag{2.4}$$

where A is a reflectivity correction factor, typically 50 to 70 dB (personal correspondence with Ms. Raisa Lehtinen, Vaisala).

Two most frequently used algorithms to estimate the PBL from wind profiler data are described in Angevine et al. (1994) and in Bianco and Wilczak (2002).

Angevine et al. (1997) detects the mixing layer height by calculating the height of the range-corrected SNR maximum for each beam. The median of the maximum of all four beams is suggested as height of the PBL. As an alternative, it is possible to calculate first the median of the range-corrected SNR profiles and then find the height of the range-corrected SNR maxima (Fig. 3.4).

Bianco and Wilczak (2002) applied the fuzzy logic algorithm to estimate the CBL height. First, clutters are removed from the signal-to-noise ratio by applying a fuzzy logic algorithm. Second, a further fuzzy logic algorithm is applied to determine CBL height, including also the variance of the vertical velocity. In this way, the true top of the CBL should be distinguished from high SNR layers aloft. The algorithm of Bianco and Wilczak (2002) is also used in the LAP-XM Boundary Layer Module (Vaisala, 2007b; Lehtinen et al., 2009). Velocity variance, spectral width, and SNR curvature and variance to estimate the CBL robustly.

However, LAP-XM Boundary Layer Module was not able to find a CBL height for the wind profiler data of CLACE2010. Therefore, the algorithm of Angevine et al. (1994) was applied on the Vaisala wind profiler data.

3.3 Planetary boundary layer height determined by COSMO-2

The numerical weather prediction model of MeteoSwiss runs at horizontal resolution of 6.6 km and 45 vertical levels (COSMO-7 (Consortium for small-scale modeling)) or at horizontal resolution of 2.2 km and 60 vertical levels (COSMO-2) (see http://www.cosmo-model.org/ for more details). Forecasts of the global model GME of the Germany's National Meteorological Service (see www.dwd.de for further informations) provide the boundary conditions for the operational runs. COSMO-2 is nested in COSMO-7 and covers the region of Switzerland. Dispersion of chemical or radioactive compounds after accidents should be modeled with the help of these COSMO models. Therefore, the models calculate also PBL height, which is an important parameter for the dispersion.

COSMO-2 calculates PBL height using the Bulk-Richardson method. PBL height is given as the height at which the Bulk-Richardson number (Ri_B) reaches the critical Richardson number of 0.33 under stable conditions (Wetzel, 1982) and 0.22 under convective conditions (Vogelezang and Holtslag, 1996).

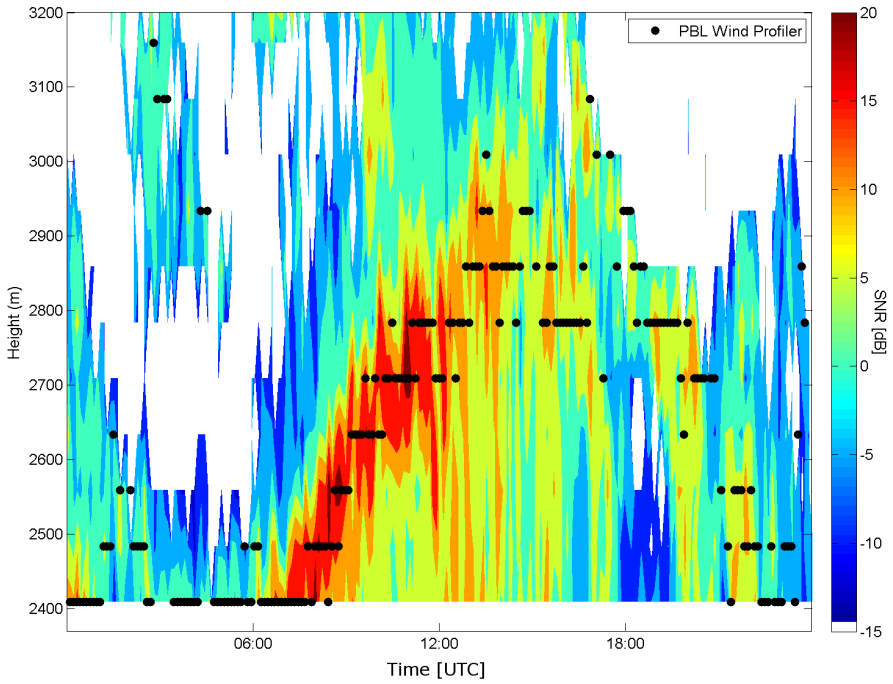

Figure 3.4: Time series of the range-corrected signal to noise ratio (SNR) measured by the wind profiler on 7 July (see color code). The retrieved planetary boundary layer height is shown (black bullets).

4 Results and discussion

4.1 Weather during CLACE 2010

A strong 'Föhn' event at the beginning of June was replaced by incoming cold air, which caused rainy weather and onset of winter above 1500 m a.s.l.. The Azores high defined the weather over Europe from end of June to mid of July. Subsidence causes adiabatic warming, high irradiation (Fig. 4.1, panel B) and air temperature (Fig. 4.1, panel C), low horizontal wind speeds but dominant vertical wind motion. During this fair-weather period convective clouds developed, leading to precipitation and thunderstorms in the course of the day (Fig. 4.1, panel E). Rain-laden and cooler weather established with sunny intervals in the second half of the July. July 2010 belongs to the fifth of the warmest months since 1864 (see "Klimabulletin" on www.meteoschweiz.admin.ch for further informations). Several fronts crossed the Bernese Alps in August 2010 causing cloudy and rainy weather and a declining snow line altitude.

The mean air temperature is 11.28°C at the KLS from 1 July to 30 August 2010 and it is 11.3°C warmer than at the JFJ. The maximal hourly averaged air temperature is 23.9°C at the Kleine Scheidegg and 10.2°C at the JFJ and the minimal hourly value is 2°C at the Kleine Scheidegg, but -12°C at the Jungfraujoch.

The wind profiler records primarily SW and secondary NE winds at 2500 m a.s.l.. Wind speed increases with height and during evening and night. With increasing height the NE component decreases and the SW component and the wind velocity increases due to reduced influence of the topography. Above around 3500 m a.s.l. wind directions from SSW to N are measured, but SW is still the most frequent direction (Fig. 2.6). The influence of Eiger, Mönch and Jungfrau on the wind field is obvious. South and southeastern wind direction up to 3832 m is rarely observed.

The Rosemount anemometer measures mainly winds from NW and rarely winds from SE (Fig. 4.2). All other wind directions are negligible. The sonic anemometer measures wind directions from NNW to E, but mainly northerly winds.

As SE wind is measured at the JFJ, the wind profiler records winds from SW. When the Rosemount pitot tube measures winds from NW the wind profiler measures W-NW wind. The wind directions are predetermined by the topography, which shows a SE-NW orientation at the JFJ and SW-NE orientation at the Kleine Scheidegg (see Fig. 4.2).

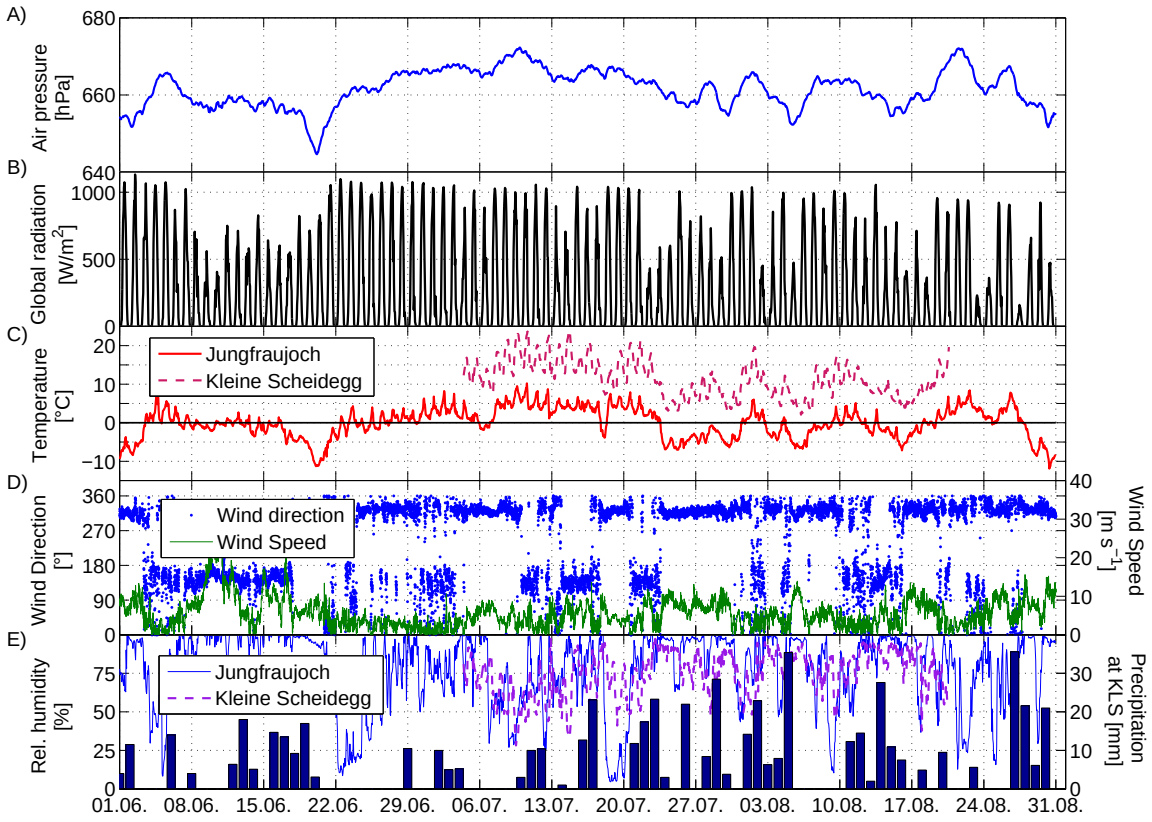

Figure 4.1: Hourly averages of air pressure (panel A), global radiation (panel B), temperature (panel C) and relative humidity (panel E) at the Jungfraujoch during CLACE 2010. Ten minutes averages of wind direction and wind speed are depicted in panel D) and in panel E) daily precipitation measured at the Kleine Scheidegg is shown.

The wind profiler measures the highest horizontal and vertical wind speed at the height of the JFJ (3533 $\pm$ 102 m a.s.l.) compared to the in-situ measurements, because the measurements are not directly influenced by surface roughness. The sonic anemometer measures rather lower horizontal wind speed than the Rosemount anemometer. However, the Rosemount pitot tube is only sensitive for wind velocity, which is higher than 2 m/s. Measurements by the sonic anemometer are highly influenced by the Sphinx, which blocks southerly winds, decelerates wind speed, causes turbulence and therefore changes wind direction. The Rosemount pitot tube and its position seems to be more appropriated for representative measurements at the JFJ, as SwissMetNet follows international standards.

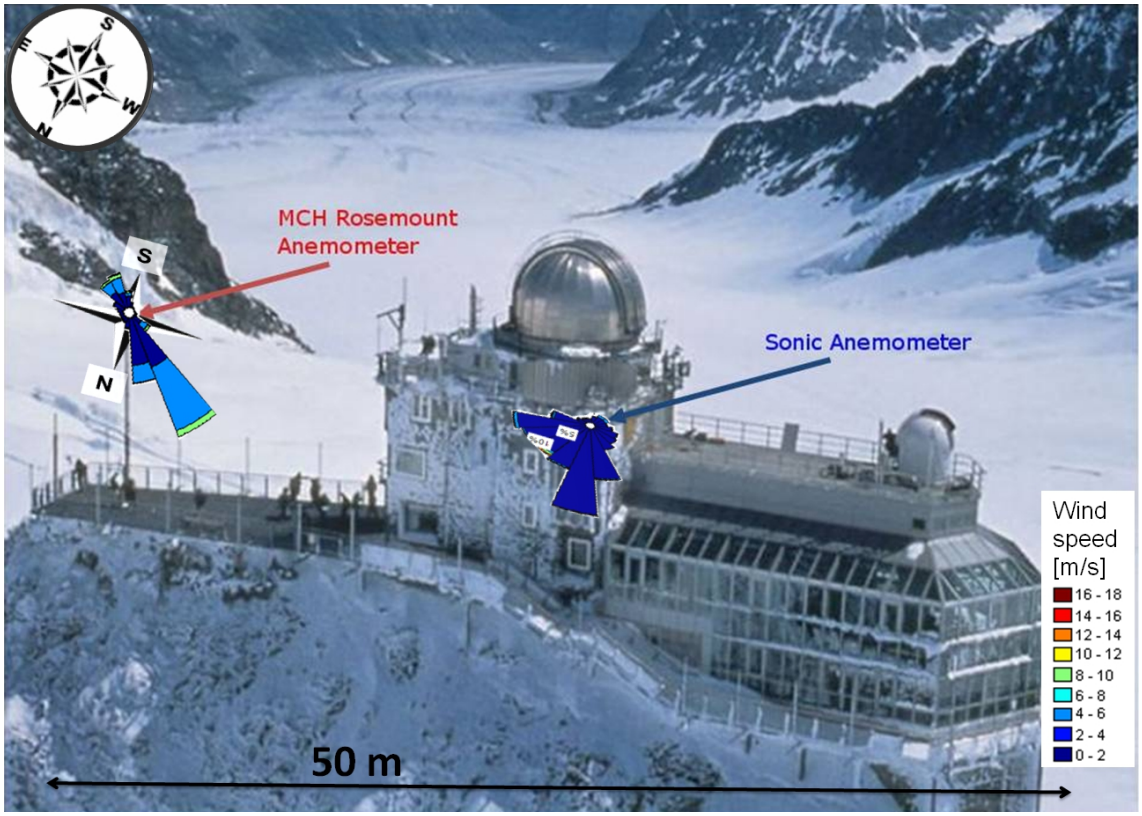

Figure 4.2: Sphinx with view to Jungfraufirn. Location of the Sonic Anemometer and the Rosemount pitot tube and the corresponding wind roses are depicted. Wind roses show the relative fraction of wind speed and corresponding wind velocity (Photo: *www.silberhorn.ch*).

4.2 Planetary boundary layer

4.2.1 Planetary boundary layer height determined using a wind profiler

The median of the maximal SNR over all beams defines the convective boundary layer height. Therefore, the maxima air density variations are analyzed. As one range gate is 75 m depth, the highest possible inaccuracies of the PBL height are ± 75 m.

The convective boundary layer (CBL) height is analyzed on following fair-weather days without precipitation or persistent cloud cover 7.7., 8.7., 9.7, 12.7, 20.7., 31.7., 7.8. and 9.8.2010 from 7 am to 20 pm. Wind profiler cannot measure during precipitation and thus CBL heights cannot be detected during periods with precipitation above the Kleine Scheidegg. The central mark of each box plot is the median, the edges of the box are the 25th and 75th percentiles, the whiskers extend 99.3 % of the data points and outliers are plotted individually (see Fig. 4.3).

The highest SNR is in the majority of cases observed at the lowest range gate at 7 am (Fig. 4.3).

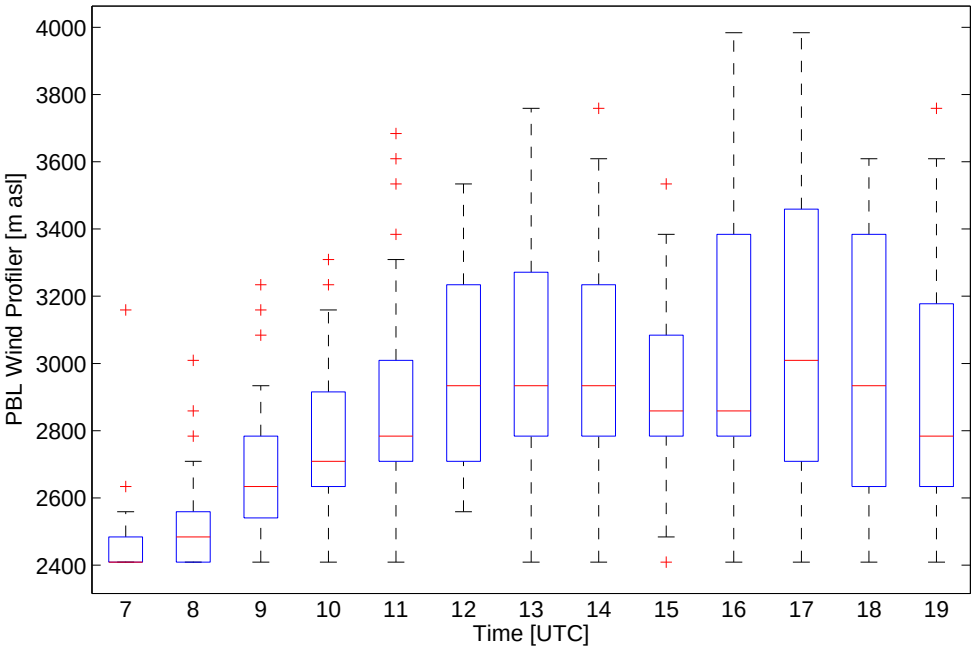

Figure 4.3: Temporal evolution of planetary boundary layer height derived by wind profiler for selected, precipitation-free days. The central mark of each box plot is the median, the edges of the box are the 25th and 75th percentiles, the whiskers extend 99.3% of the data points and outliers are plotted individually. Only days without precipitation and without persistent cloud cover come into consideration for the analysis of the planetary boundary layer height.

The CBL height starts to increase and peaks at around 2900 m a.s.l. and th 75th percentile at 3500 m a.s.l. at noon. The average growth is 130 m per hour from 7 am to 1 pm. The highest median of the CBL height is measured at 2 pm, but the highest maximum and 75th percentiles value is observed at 1 pm over the Kleine Scheidegg. The CBL height depicts a plateau in the afternoon. The variability of the data points increases about noon, due to individual growing rates during different days. The standard deviation decreases at 3 pm and increases again about late afternoon. This increase is caused by a decreasing height of the convective boundary layer and the observation of a second descending layer of maximal SNR. This second descending layer might be formed due to change in vertical wind velocity and wind direction in the evening (further description see section 4.3).

The progress of the CBL height of the single days can be seen in Fig. 4.4.

The highest planetary boundary layer top is detected on 12 July and the lowest on 7 August 2010. A period of days with fair-weather, less precipitation and clouds from 7 July to 12 July leads to increasing PBL height over those days. On 9 August and 20 July an increase of the mixing layer height occurs about evening. During all other days, a second layer is detected in the late afternoon, whose height decreases rapidly similar to the first decreasing layer.

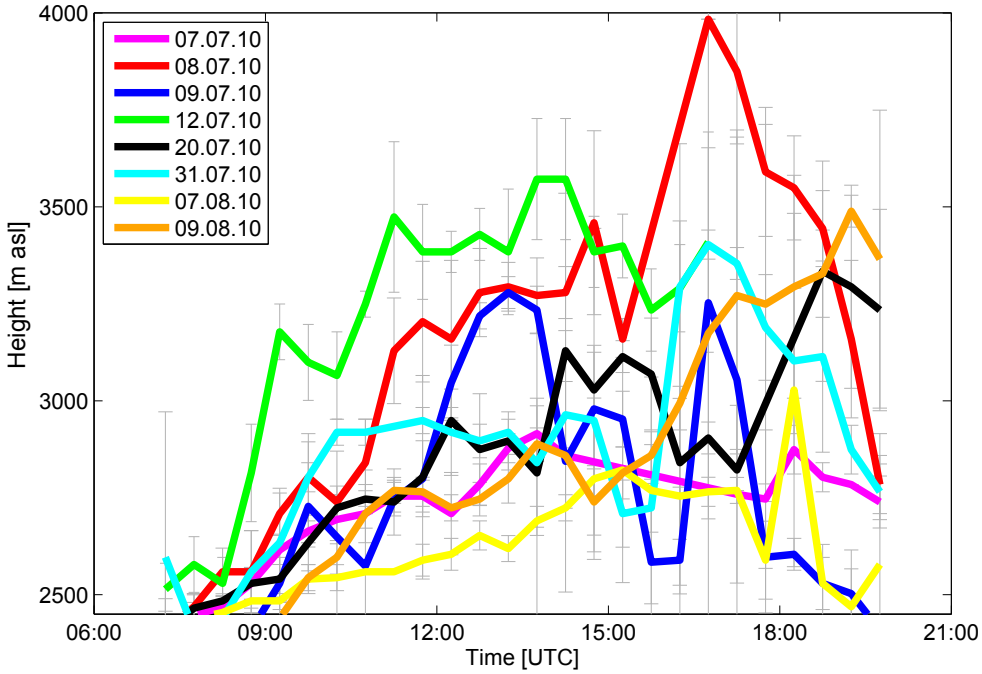

Figure 4.4: Diurnal cycle of the planetary boundary layer height determined by the wind profiler. Grey error bars denote the standard deviation hourly values.

4.2.2 Planetary boundary layer height determination using a ceilometer

Different aerosol layers are detected by the ceilometer. To analyze the PBL height the lowest layer depicts the convective boundary (Fig. 4.5 panel A) layer during daytime and a second residual layer is of importance during evening and night (Fig. 4.5 panel B) during the fair-weather days 7.7., 8.7., 9.7, 12.7, 20.7., 31.7., 7.8. and 9.8.2010.

The first aerosol layer varies from midnight to 7 am in the morning. Median decreases from approximately 2750 m a.s.l. at 2 am to 2450 m a.s.l. at 7 am. After 7 am the PBL height rises and a maximal median value of 3000 m a.s.l. and the maximum of 3500 m a.s.l. are measured at 2 pm. The PBL height decreases in the afternoon to median value of 2400 m a.s.l. at 9 pm. The average increase of the PBL is about 500 m in during fair-weather days.

The second aerosol layer possesses a larger distribution of values with fewer points. A second decreasing layer above the CBL is sometimes present in the afternoon. From 3 pm to 8 pm the height of the second layer decreases as well as the median vertical difference between both layers from $\Delta h = 540$ m to $\Delta h = 315$ m. The interquartile range is very large with values up to 900 m, especially during evening, but also during night. From 3 am to 7 am the second layer is decreasing similarly to the lower layer.

Single planetary boundary layer heights on fair-weather days are shown in Fig. 4.6. Most of

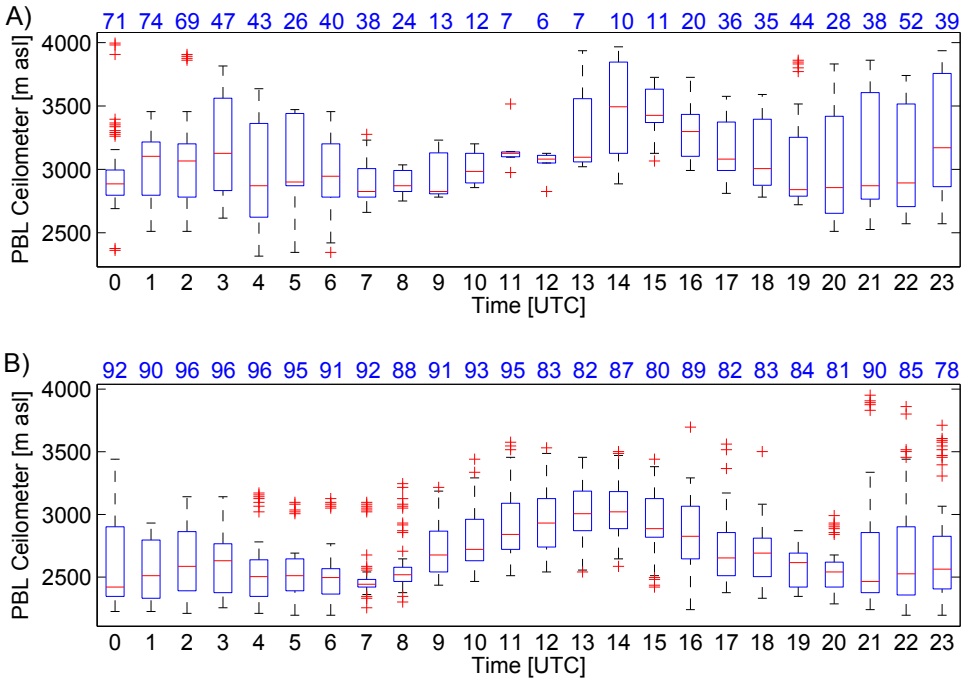

Figure 4.5: Box plots of diurnal cycles of the planetary boundary layer height determined by the ceilometer. Panel A), second aerosol layer height(residual layer) and panel B) lowest aerosol layer height (lower residual layer and daytime PBL). The central mark of each box plot is the median, the edges of the box are the 25th and 75th percentiles, the whiskers extend 99.3% of the data points and outliers are plotted individually. Only discussed days are evaluated and the number of points are represented by the blue number above each box plot.

the PBL show a decrease during night with a minimum in the morning, before the mixing layer height increases to 2600 to 3500 m a.s.l.. The mixing layer heights decrease again in the afternoon.

However, on 12 July 2010 after precipitation, data are meanwhile not available, the lowest aerosol layer is detected above 3900 m a.s.l.. Thereby, the gradient between aerosol concentration in a cloud and above a cloud is marked as a PBL height. On 9 July the mixing layer height also increases in the evening. On this day Sahara dust crests the Jungfraujoch and perturbs the measurements.

4.2.3 Comparison the planetary boundary layer height algorithms determined by different algorithms and instruments

In this section, Jenoptik and STRAT-2D algorithms are compared, as well as the PBL height determined using the wind profiler and the ceilometer.

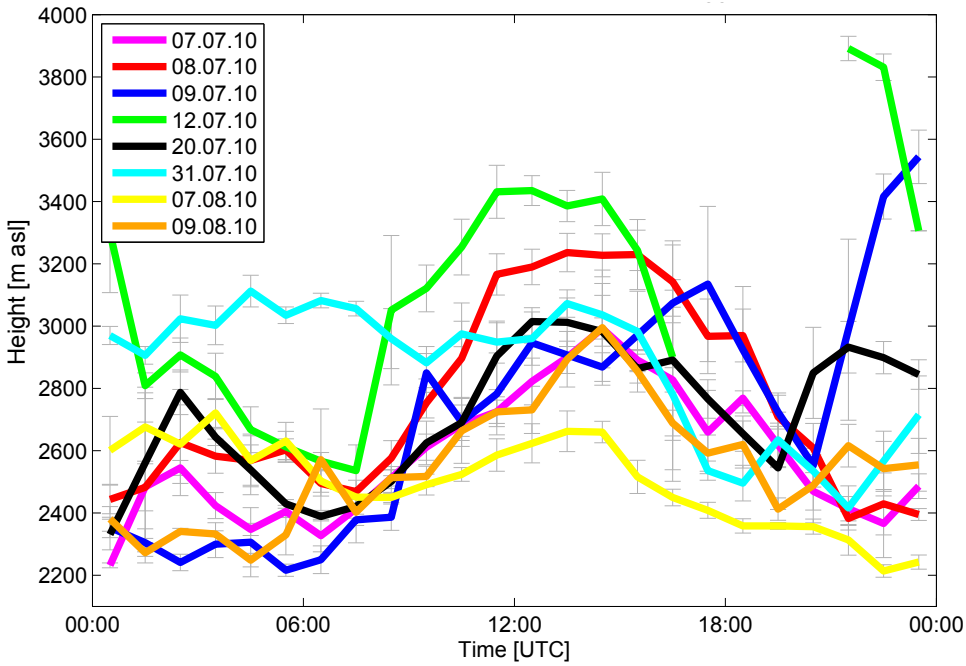

Figure 4.6: Temporal evolution of the lower level of the planetary boundary layer height determined by the ceilometer. Grey error bars denote the standard deviation of each hour.

First, two algorithms for ceilometer, STRAT-2D and Jenoptik, are compared on the fair-weather days 7.7., 8.7., 9.7, 12.7, 20.7., 31.7., 7.8. and 9.8.2010 over daytime and over the whole day.

STRAT-2D algorithm estimates a higher PBL than Jenoptik (Fig. 4.7). PBL height shows an offset of 220 $\pm$ 76.3 m over daytime and -120 $\pm$ 46 m over the whole day. R-squared is 0.8 over daytime and $R^2 = 0.7$ over the whole day. The larger difference during evening and night is due to two residual layers. They are not always detected by both algorithms in the same dataset.

For the following linear regressions (Fig. 4.7, 4.8) a bivariate weighted fit (York et al., 2004) is used. This method takes the uncertainties of x and y variables into account.

Planetary boundary layer height is determined using the wind profiler and the ceilometer on the fair-weather days 7.7., 8.7., 9.7, 12.7, 20.7., 31.7., 7.8. and 9.8.2010 over daytime, because the wind profiler is only suited to estimate PBL heights during daytime (Angevine et al., 1997). Between sunset and sunrise the strongest range-corrected SNR is often detected in the lowest range gate.

While the ceilometer uses gradients in the aerosol backscatter, the wind profiler uses gradients in the refractive index, which is reflected in the range-corrected SNR. This means the ceilometer detects aerosol layers (AL) but the wind profiler detects CBL.

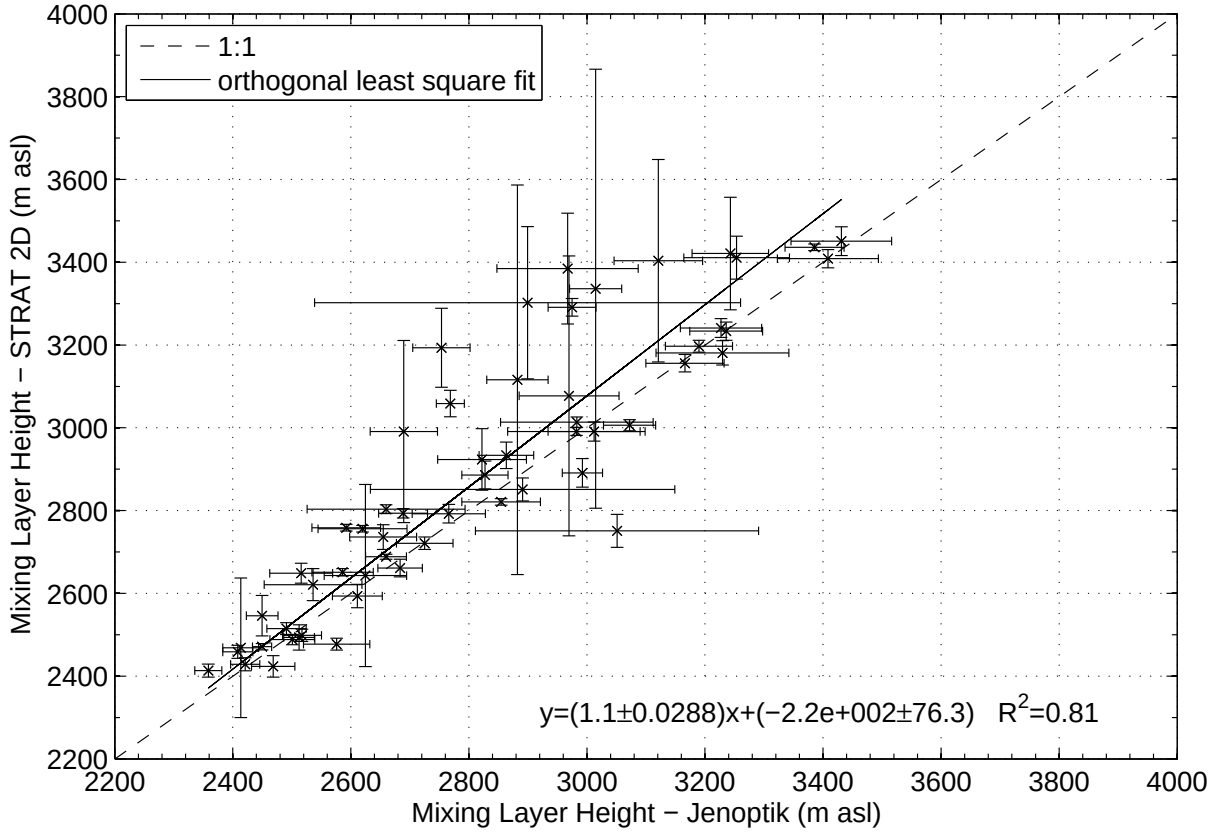

Figure 4.7: Comparison of PBL algorithms Jenoptik and STRAT-2D on the defined fair-weather days over daytime.

Nevertheless, the ceilometer AL and the wind profiler CBL agree well, especially for periods without clouds (Fig. 4.8). The slope of the linear regression is around 1 (0.99 and 1.02) for all data and for PBL under clear sky. Thereby, the regression coefficient is R^2=0.7 for all data and R^2=0.8 for PBL under clear sky. Points which deviate from the slope have large standard deviations. The too high wind profiler points under clear sky conditions can be explained by the fact that the wind profiler measures often a second decreasing layer in the late afternoon, which is higher than the AL measured by the ceilometer.

Comparing the PBL height of both instruments under cloudy conditions results in a slope of 0.89 and an offset of 310 ± 215 m with R^2 of 0.4. The average difference between planetary boundary layer determined by ceilometer minus planetary boundary layer determined by wind profiler is -94.89 m under cloudy and -34.06 m under clear sky conditions (see Fig. 4.9). The mean difference of the two instruments is around-34 m.

Both instruments, ceilometer and wind profiler have problems to differentiate between clouds and PBL height. The ceilometer often identifies the aerosol gradient between cloud and sky above as PBL. The refractive index is maximal above clouds, due to the large gradient of humidity and turbulence, as well as the occurrence of wind shear above the cloud top (Grimsdell

and Angevine, 1998; Bianco and Wilczak, 2002). Moreover, cloud tops can occur below the PBL top, in the entrainment zone, or above the PBL (Stull, 1988). This complicates the interpretation and a possible improvement of algorithms.

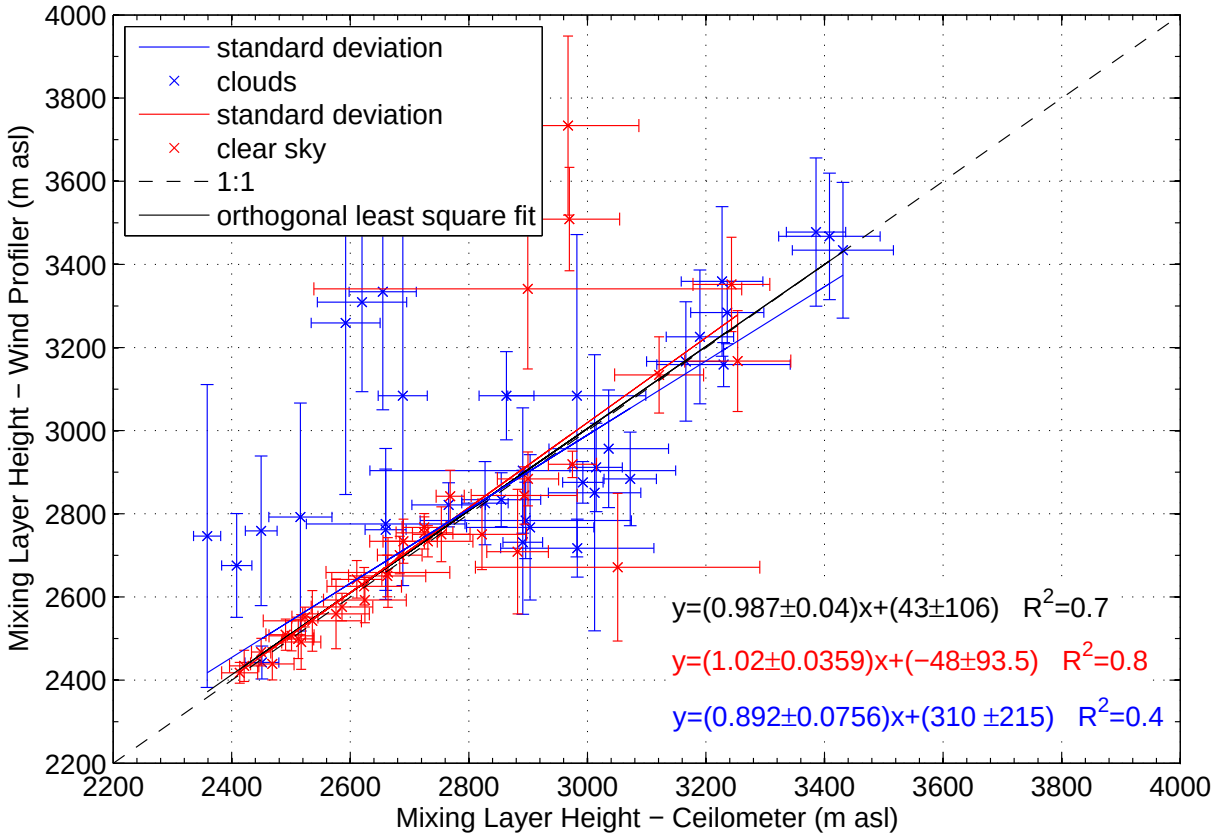

Figure 4.8: Comparison of ceilometer with wind profiler planetary boundary layer height classified into cloudy or clear sky conditions on the fair-weather days during CLACE2010. Hourly averaged data are used. For ceilometer data the averaged quality index has to exceed 2.2, so that mainly data points with weak and good quality are considered.

Although ceilometer detects aerosol layer height but wind profiler estimates the convective boundary layer height, the results agree well, especially for periods without clouds.

However, "[...] considerably differences between CBL and AL" are described by de Wekker et al. (2004). The convective boundary layer is described in literature from a CBL that follows the terrain (de Wekker et al., 2004) to a CBL which is uncoupled from the terrain (Kossman, 1998). In contrast, an AL is nearly uniform in height and generally does not follow the underlying terrain on a scale up to tens of kilometers (Nyeki et al., 2000; de Wekker, 2002). A difference in height between AL and CBL exists, which changes over the day. In the morning, Convective boundary layer height follows the terrain during the morning, while the aerosol layer can be 1-2 km higher than the CBL in a valley. As convective boundary layer grows, the difference between CBL and AL height becomes smaller until the CBL grows faster than the AL

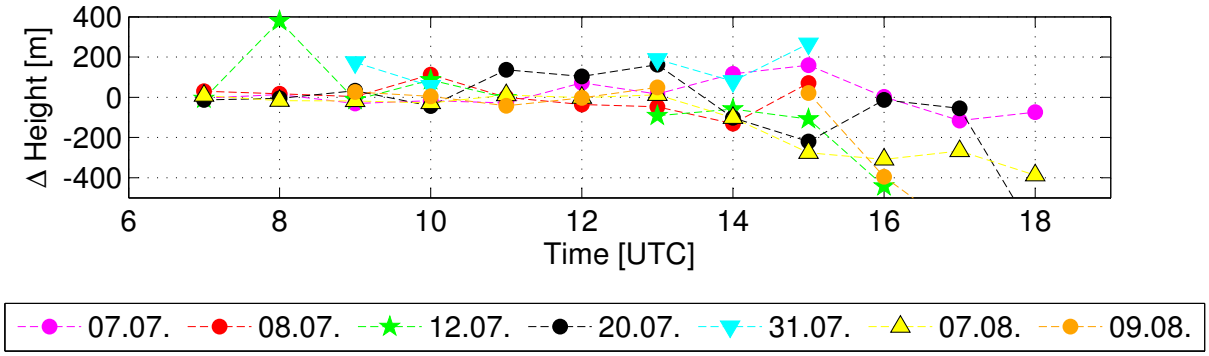

Figure 4.9: Diurnal cycle of differences between planetary boundary layer determined by ceilometer minus planetary boundary layer determined by wind profiler (ceilometer PBL height - wind profiler PBL height) on the defined days over daytime.

between 12 and 15 UTC. After 15 UTC CBL and particle layer heights gradually decreases as convective processes become weaker and subsidence begins to dominate (de Wekker et al., 2004).

The differences between PBL height derived by the ceilometer and the PBL height derived by the wind profiler agree well over daytime, but differ in the evening (Fig. 4.9). The results of the comparison between wind profiler and ceilometer PBL height in this study show, that AL and CBL height show a similar behavior at the Kleine Scheidegg over daytime.

4.2.4 Comparison of planetary boundary layer determined by in-situ and remote sensing measurements

The diurnal cycle of particle number concentration N, scattering coefficient σ_{sp} (450 nm) and absorption coefficient σ_{ap} (470 nm) is shown in Fig. 4.10. Particle number concentration is dominated by the Aitken mode and therefore characterizes the formation and growth of new particles from gaseous precursor (Collaud-Coen et al., 2011). The daily cycle of the aerosol number concentration has its minimum of N=207 cm^{-3} at 6 am with a median of 457 cm^{-3} and increases to a maximum of 2225 cm^{-3} at 2 pm. Spikes of σ_{ap} and N, usually between 7 and 10 am, correspond to local pollution events, due to snow groomer and other touristic activities. Important parameters for new particle formation explain the diurnal cycle of N. Solar radiation, low temperatures, high precursor concentration but low aerosol surface area concentration are important for this process. From 2 pm to 6 pm the aerosol number concentration decreases again and the median varies around 500 cm^{-3} during night. Air from free troposphere replaces the ambient air at the JFJ around 10 pm, which is reflected in a sharp decrease of aerosol number concentration.

The scattering coefficient is minimal at 6 am in the morning, increases until 3 pm, where a maximal median of $2.7 \cdot 10^{-5}$ m^{-1} occurs and at 4 pm the absolute maximum of $3.6 \cdot 10^{-5}$ m^{-1}.

Then the scattering coefficient remains on this high level until 10 pm.

The absorption coefficient is characteristic for pollutant air masses, as it is sensitive to BC concentration. The absorption coefficient is minimal at 5 am and it increases until 4 pm. The absorption coefficient stays on a high level during the afternoon and evening until 11 pm. During the night absoption coefficient decreases, because the air mass is replaced by free troposphere air.

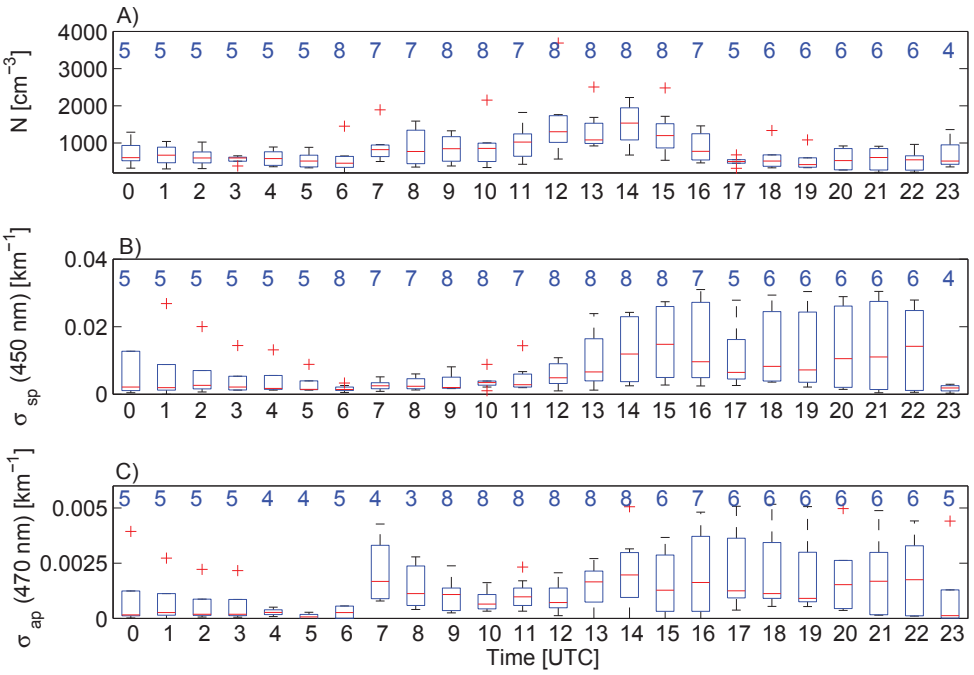

Figure 4.10: Box plots of the diurnal cycle of the median, 25th and 75th percentiles and outliers of the particle number concentration N (panel A), aerosol scattering coefficient σ_{sp}(panel B), and aerosol absorption coefficient σ_{ap} (470 nm) (panel C) measured at the Jungfraujoch. Only the discussed fair-weather days are used and the data are averaged over one hour. The blue number above each box plot represents the number of points. Outliers caused by building and tourism activities are removed.

The in-situ aerosol number concentration N, scattering coefficient σ_{sp} (470 nm) and absorption coefficient σ_{ap} (470 nm) are now compared with PBL height estimations of remote sensing instruments on fair-weather days during CLACE2010.

Figure 4.11 shows an example of PBL heights derived by the remote sensing instruments ceilometer and wind profiler over the Kleine Scheidegg and the in-situ measurements of scattering and absorption coefficient on the Jungfraujoch on 12 July 2010. The first plot shows the ceilometer range-corrected backscatter signal and the PBL corresponding to the gradients of Pr^2. Two residual layers seem to decrease from midnight to the early morning. Planetary boundary layer increases to about 3500 m a.s.l. any time in the morning. Convective clouds develop along the

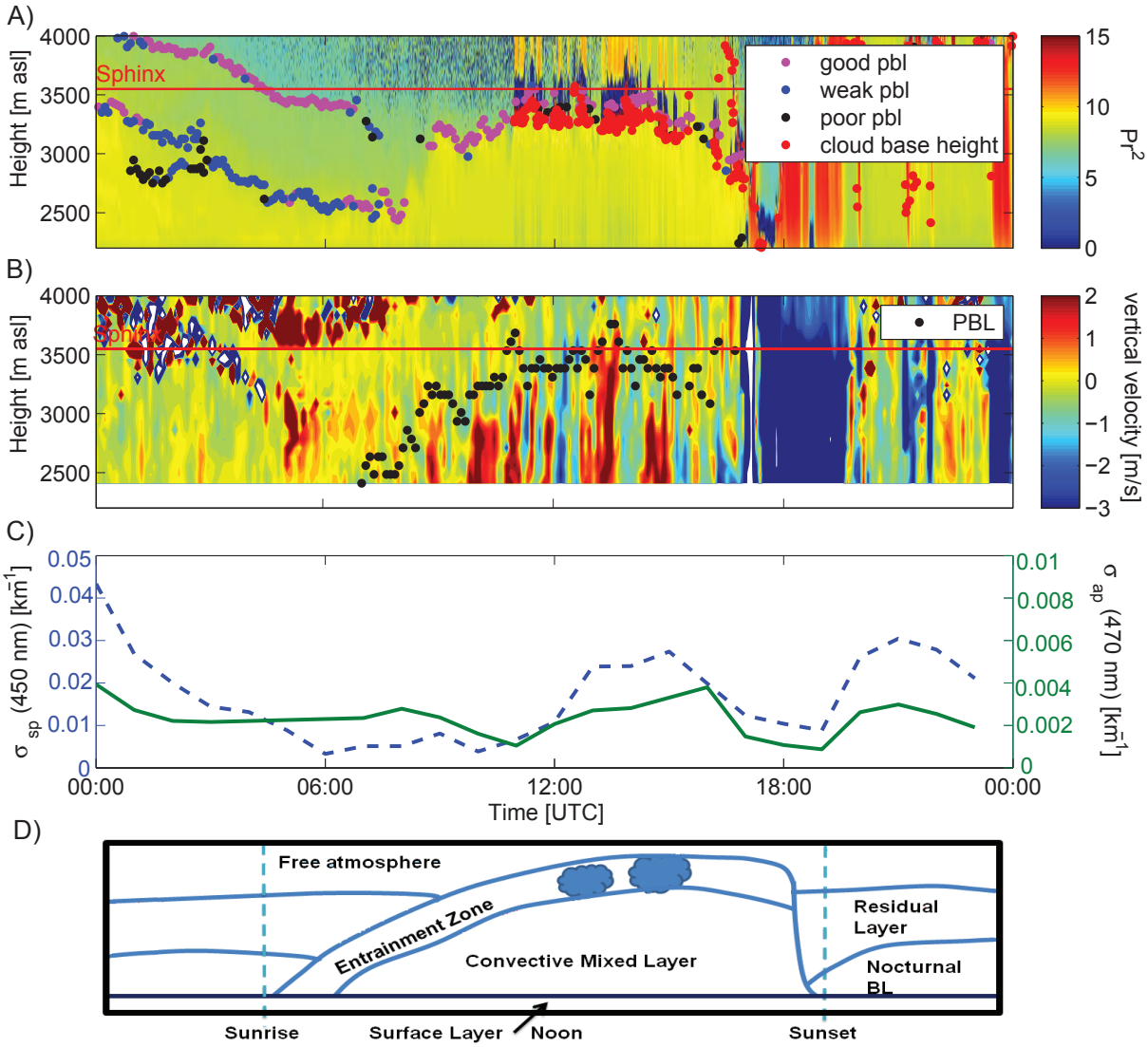

Figure 4.11: Panel A) ceilometer range-corrected backscatter (Pr^2) and planetary boundary layer height determined using Jenoptik algorithm and cloud base height (red dots) on 12 July 2010. Panel B) planetary boundary layer determined by wind profiler (black dots) and vertical velocity. Positive values of vertical velocity show updraft and negative values downdrafts. Scattering coefficient and absorption coefficient measured at the Jungfraujoch are depicted in panel C). Panel D) typical diurnal PBL cycle, after Stull (1988), modified. The red line depicts the height of the in-situ measurements at the Sphinx.

PBL top at noon and in the afternoon, before precipitation sets in. The planetary boundary layer height derived by both remote-sensing instruments are in good agreement over daytime. Thermals and updraft plumes can be observed in the vertical velocity, which is strong with values up to 2 m/s from 8 am to 3 pm.

Scattering and absorption coefficients show strong decrease from midnight to 6 am. This corresponds with aerosol layers, which also decrease in height. The scattering coefficient and absorption coefficient increases until 3 pm and 4 pm, decrease during the precipitation and increase again in the evening.

Two aerosol layers decrease from midnight to 7 am. The planetary boundary layer deepens sharply with a maximum at about 1 pm. In the afternoon the PBL height decreases and does not stay at the same height as shown in the scheme of Stull (1988). Precipitation and clouds inhibit further reliable detection of the PBL.

Injections of the planetary boundary layer are measured at the JFJ on 08.07.-09.07., 12.07.2010 and 20.07.2010 during the afternoon. This is reflected in the absorption and scattering coefficient (Fig. 4.12). On the contrary, PBL stays below 3200 m a.s.l. on 7 July, 31 July and 7 August and neither absorption nor scattering coefficient increases so that no PBL air reaches the JFJ (Fig. 4.13). Increase in number of particle during the same day is due to new particle formation and subsequent growth.

When we consider single days, a relation between PBL height and in-situ measurements is evident. On 8 July 2010, the PBL has a maximum of 3250 m a.s.l. over the Kleine Scheidegg at 1 pm. Absorption and scattering coefficients increase to a maximum at 6 pm (Fig. 4.12).

After 6 pm they decrease rapidly to a low, nocturnal level. Injections of the PBL are measured at the Jungfraujoch, although the measured PBL height above the Kleine Scheidegg is 300 m lower than the Jungfraujoch. The transport of PBL air upwards can be explained by strong updrafts, which are also measured by the wind profiler (see example of 7 July, Fig. 4.17).

On 9 July 2010 the diurnal PBL rises less to about 3200 m a.s.l., but in the evening an increasing aerosol layer is detected, which is also visible in the scattering and absorption coefficient. On 9 July Sahara Dust is present at the Jungfraujoch. The Sahara dust event starts at 9 am and ends on 10 July at 9 am. During the day the Sahara dust sinks down to the Jungfraujoch, where it can be observed. Scattering and absorption coefficient do not decrease as on 7 July, but stay at a high level until midnight. The aerosol layer detected by the ceilometer in the later evening might be a gradient above the Sahara dust.

The ceilometer indicates a very high PBL up to 3450 m a.s.l. on 12 July 2010 between 11 am and 2 pm. The absorption and scattering coefficient increases to a maximum at 5 pm, before precipitation started. During precipitation the aerosols are scavenged. Afterwards, absorption and scattering coefficient increase again to a similar level than before, because another air mass arrived at the JFJ, where the particles have not been scavenged.

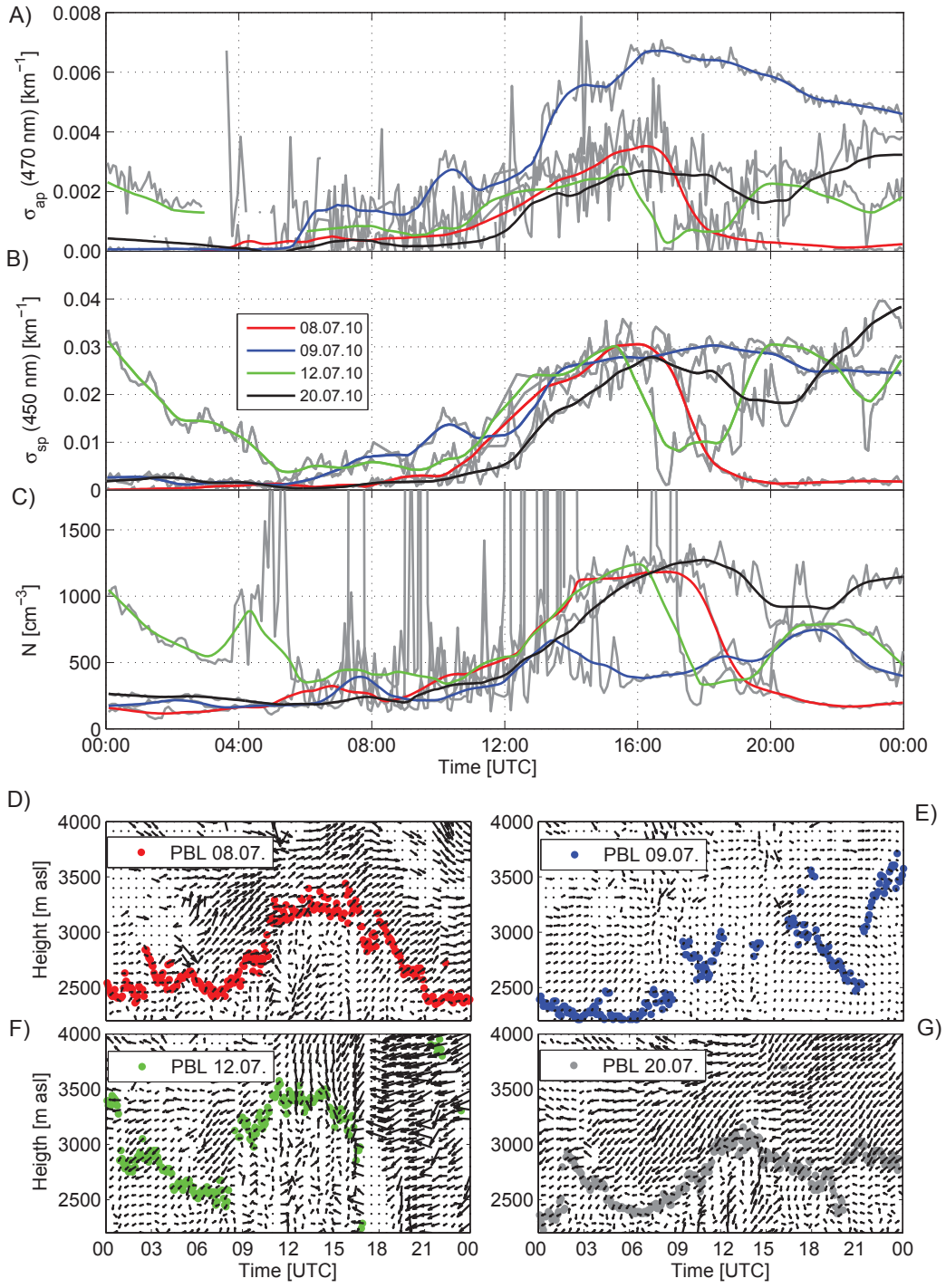

Figure 4.12: Time series of absorption coefficient (panel A), scattering coefficient (panel B), aerosol number concentration (panel C) measurements. The colored lines show smoothed data over two hours without spikes and the grey lines denote the raw data for selected days (see legend). Panel D-G) corresponding wind direction and wind speed (measured by the wind profiler) and planetary boundary layer height (derived by Ceilometer, Jenoptik retrieval).

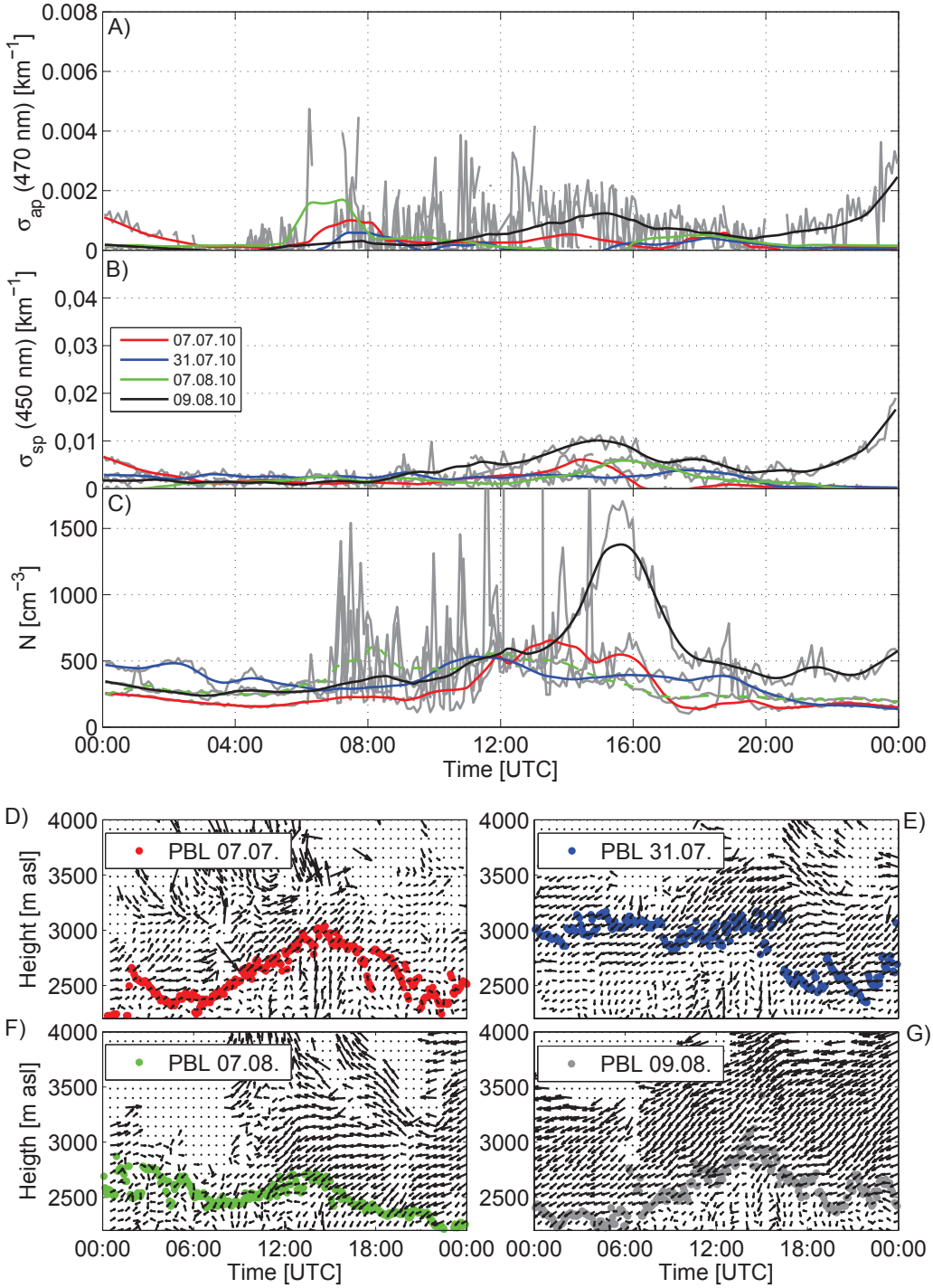

Figure 4.13: Time series of absorption coefficient (panel A), scattering coefficient (panel B), aerosol number concentration (panel C) measurements. The colored lines show smoothed data over two hours without spikes and the grey lines denote the raw data for selected days (see legend). Panel D-G) corresponding wind direction and wind speed (measured by the wind profiler) and planetary boundary layer height (derived by Ceilometer, Jenoptik retrieval).

On 20 July 2010, the values of scattering and absorption coefficient stay at a high level in the evening and also the residual layer almost stays at the same altitude as at noon, as depicted in the scheme of Stull (1988) in Fig. 4.11.

Low pressure areas are always present over the Alps, when injections of the PBL are observed at the Jungfraujoch during CLACE2010. The Schüepp synoptic weather type of the Alps (SYNALP) classification from the Alpine Weather Statistics (Schüepp, 1979) is used to define the synoptic meteorology over Switzerland over these days. The dominant SYNALP weather type is convective indifferent or convective anticyclonic on the defined fair-weather days with pronounced diurnal cycle of the planetary boundary layer. Convective weather types describe a dominant vertical motion and subordinated horizontal wind. This finding corresponds with the results of Collaud-Coen et al. (2011).

In Fig. 4.14 Jenoptik PBL height above the Kleine Scheidegg is compared with scattering coefficient and absorption coefficient.

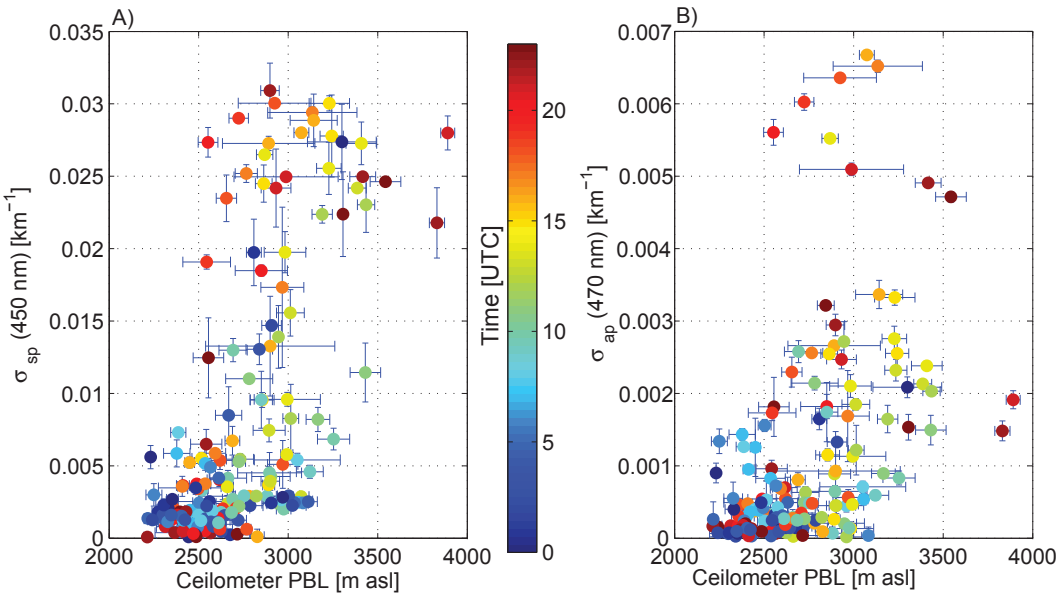

Figure 4.14: Scattering and absorption coefficient versus planetary boundary layer height derived using the ceilometer above the Kleine Scheidegg on described fair-weather days. Standard deviation of the planetary boundary layer height and scattering and absorption coefficient are depicted. The color of the single scatter points represents the daytime.

However, scattering coefficient is influenced by photochemical processes, which depend on air temperature and radiation. Therefore, a scattering coefficient implies a certain error, when taken as an indicator for PBL air. Also under FT conditions the values of the scattering coefficient peak in the afternoon.

The relation between PBL height and absorption coefficient is not very clear. During night and in the morning PBL height and absorption coefficient are below 300 m and $2{\cdot}10^{-6}\,m^{-1}$. When the PBL height exceeds 3200 m, the absorption coefficient increases above $1{\cdot}10^{-6}\,m^{-1}$, which takes place after 2 pm. One can conclude, that if the aerosol layer is higher than 3000 m injections of the PBL are transported upward by slope winds towards the Jungfraujoch.

4.2.5 Comparison of planetary boundary layer determined by COSMO-2 and ceilometer

The comparison between PBL height determined by the diffusion model COSMO-2 and measured PBL height over the Kleine Scheidegg is of special interest, to verify the simulated PBL height in alpine regions. There are no continuous measuring instruments installed, which could be used to study the PBL height in the Swiss Alps.

Planetary boundary layer heights of COSMO-2 are compared with the planetary boundary layer height determined using the Jenoptik algorithm for ceilometer data on the defined fair-weather days and with the planetary boundary layer height determined using the wind profiler on the described days over daytime from 7 AM to 6 PM.

Two points of the COSMO model are used for the comparison of PBL height derived by remote sensing measurements and PBL height simulated by COSMO-2 at the Kleine Scheidegg. The first point is defined at longitude of 7.963, latitude of 46.582 and on an altitude of 1956 m. The second point lies at long. 7.962, lat. 46.602 and on a height of 1752.8 m. They differ in height and surface type, while the surface type of the first point is rock, the surface type of the second grid point is ice. The surface type of grid point influences e.g. the temperature and humidity profile due to their albedo, water content, roughness and other characteristics. And these two parameters are important to calculate the Bulk-Richardson number.

The planetary boundary layer height of the first point shows a clear negative offset of 570 m to the PBL height derived by the ceilometer and a slightly biased negative offset of 730 compared to the wind profiler PBL. The correlation coefficients are 0.3 for the comparison with the ceilometer derived PBL height and 0.1 for the comparison with the PBL height estimations using the wind profiler. The root-mean-square error (RMSE) is 655 m and 739 m. The comparison with the second point shows a strong biased negative offset (Fig. 4.15) with weak correlation coefficients of 0.3 and 0.2. The root-mean-square error for the comparison between PBL height simulated by COSMO-2 and PBL height estimations using the ceilometer is 552 m and between wind profiler and COSMO-2 522 m.

COSMO-2 is thus not suitable to determine the PBL height in mountainous regions.

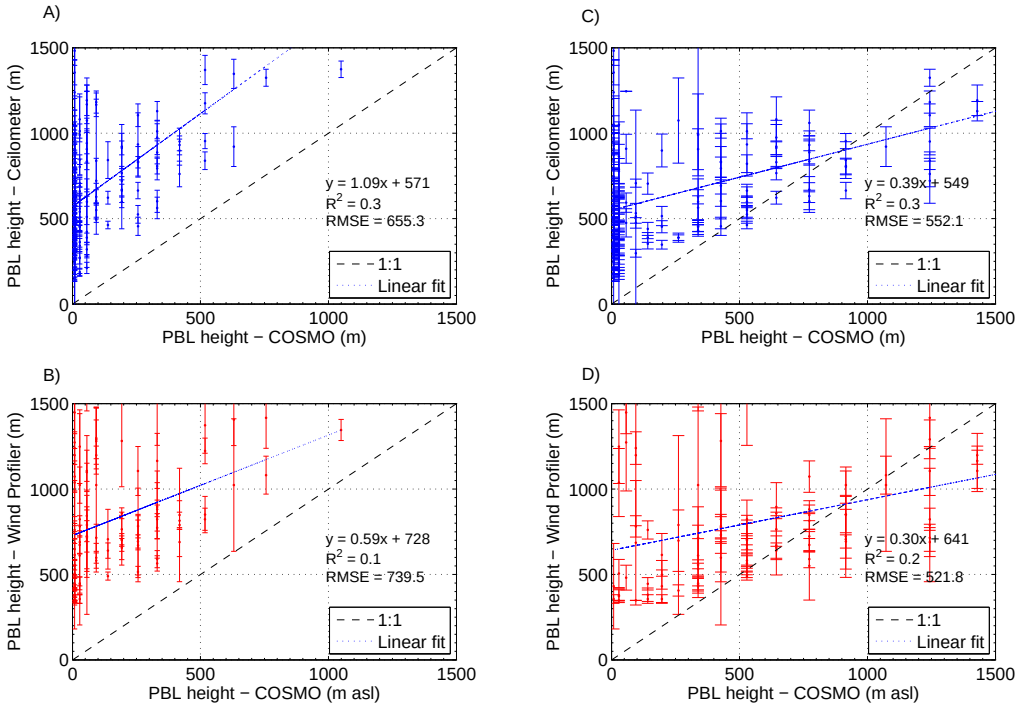

Figure 4.15: Comparison of the planetary boundary layer height simulated using COSMO-2 and determined using the ceilometer on the fair-weather days over daytime. Two grid points are used to represent the conditions of the Kleine Scheidegg. The first point is defined at longitude of 7.963, latitude of 46.582 and at a height of 1956 m. Panel A) planetary boundary layer height of the first grid point compared with the height determined by the ceilometer. The second point lies at long. 7.962, lat. 46.602 and at a height of 1752.8 m. Panel C) planetary boundary layer height of the second point is compared with the PBL height derived by the ceilometer. PBL heights derived by COSMO-2 and measured by wind profiler are compared for grid point one (panel B) and grid point two (panel D). The planetary boundary layer heights are above grid point and above Kleine Scheidegg. For every comparison the linear fit, correlation coefficient and root-mean-square error (RMSE) is depicted.

4.3 Case study of planetary boundary layer and wind field at the Kleine Scheidegg

On 7 July 2010 a high pressure area is situated over Germany and a low pressure area is situated over the Central Alps (Fig.4.16).

Northerly winds are observed by the wind profiler above 3500 m (Fig. 4.17, while SE winds are measured in lower altitudes.

In the morning after 6 am strong updrafts are observed between 2700 m and 3200 m height. Additionally, SNR has very high values at 3350 to 3600 m altitude during the same period. High SNR indicates turbulence and strong variations of humidity and temperature. This high

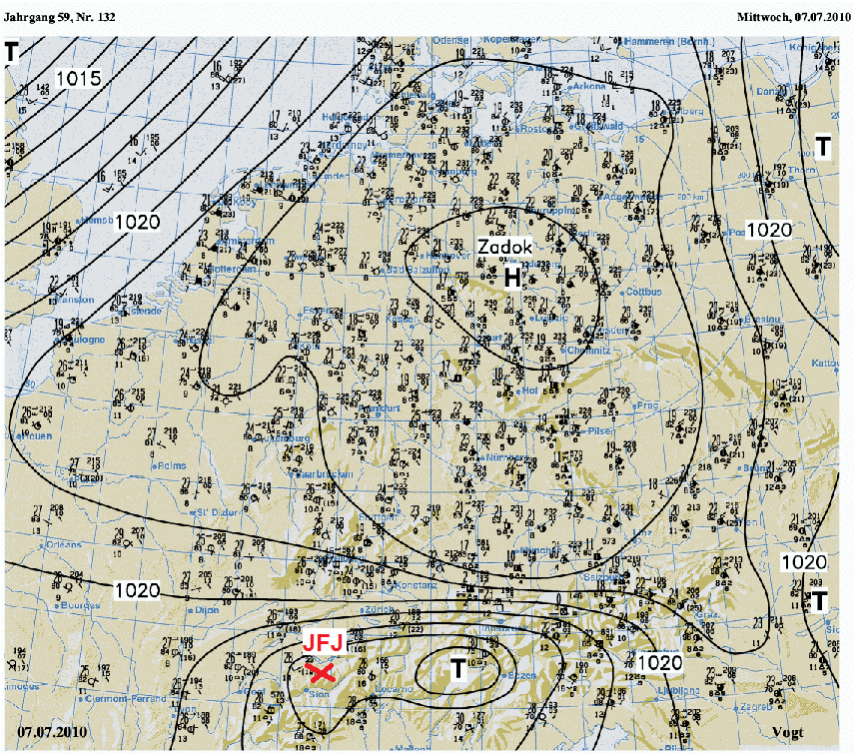

Figure 4.16: Weather map for middle Europe on 7 July 2010 (Berliner Wetterkarte, taken from http://wkserv.met.fu-berlin.de/). Isolines depict isobars, which are lines of equal pressure. Low pressure areas are located above the Eastern Alps and a high pressure above Eastern Germany.

SNR reflects an area with strong wind shear, where northerly winds meet southwesterly winds. The area with strong updraft was first suggested to be noise. However, these updrafts occur on several days of the campaign. The updrafts are decoupled from the surface, therefore we can suggest, that they are not thermally induced. Another suggestion is, that the updrafts might be induced by mountain wave activity, caused by strong northerly winds crossing the Lauberhorn-Männlichen range (Fig. 4.18). It might be a standing lee wave, which breaks after some hours. Certainly, the north face of Eiger might also force N winds to overflow its peak, and triggers updrafts. However, these strong updrafts cannot always be seen during periods with northerly wind. For this reason, a stable, breaking mountain wave is concluded as a reason for this strong updrafts.

In the course of the day several decoupled wind systems form: First the gradient wind from north above 3500 m a.s.l., second thermal induced SW winds and third the pronounced regime of the planetary boundary layer with strong updrafts during daytime. These decoupled wind systems might also have a certain influence on wave activity.

Two decreasing aerosol layer can be seen from midnight to 6 am. These two residual layers are

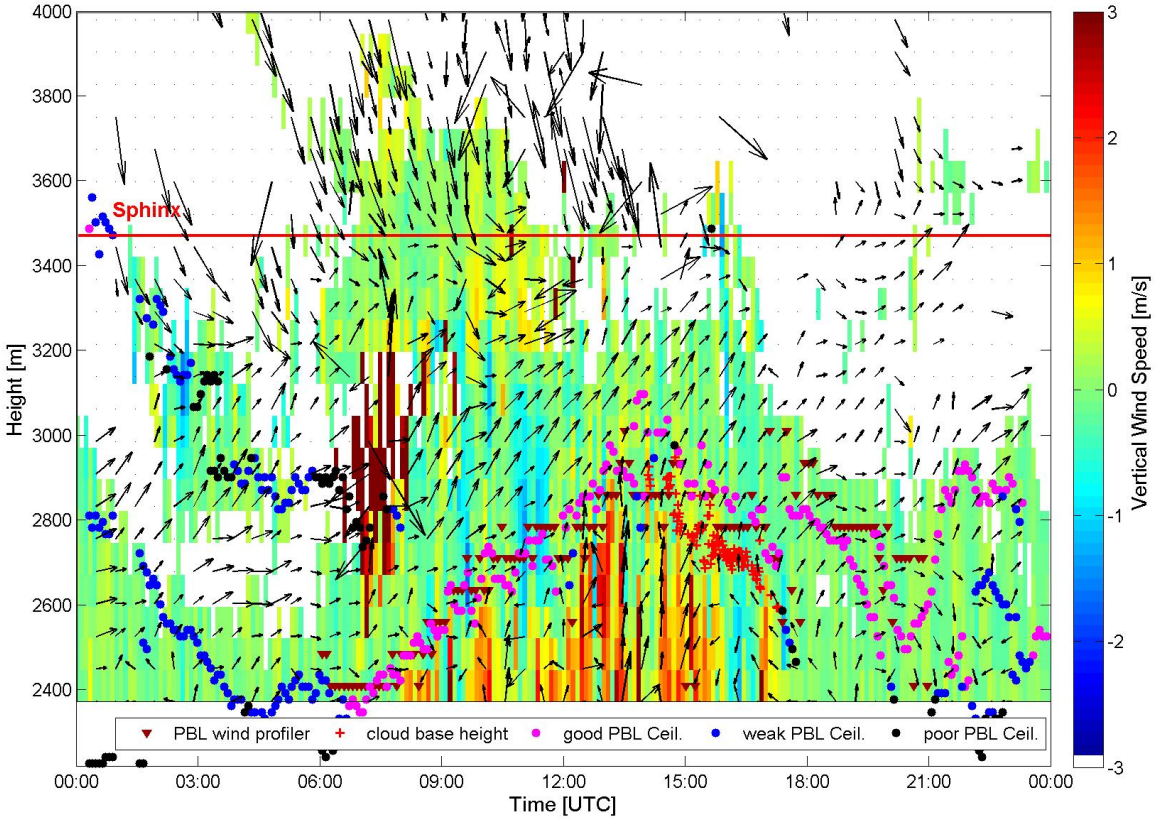

Figure 4.17: Vertical wind velocity (see color bar), horizontal wind velocity (length of arrows) and wind direction (orientation of arrows), measured by the wind profiler on 7 July 2010. Planetary boundary layer height determined by ceilometer and indexed according the quality index (points, color see legend), determined by wind profiler (dark red triangles) and cloud base height (red crosses) measured by the ceilometer are shown.

interpreted as two histories of former days. After sunrise, at 7 am the boundary layer starts to rise rapidly until 2 pm. After 5 pm two declining layers are observed by the ceilometer and the wind profiler. The development of two declining layers in the afternoon is not easy to explain (Fig. 4.17). Generally not much is known about the decay of the PBL (Pino, 2011). Schematically, a residual layer remains at the same height as the PBL reaches in the afternoon and a second, weak decreasing layer can be seen. The mixing layer decays due to the ceasing turbulence. Together with the decay of the turbulence the lapse rate in the stable boundary layer changes to a stable condition. Probably the decay of the PBL at KLS is influenced by the mountain-valley circulation. As Kleine Scheidegg is a saddle between Lauterbrunnen and Grindelwald, slope and probably also valley winds from Lauterbrunnen and Grindelwald are present. W to SW winds are continuously present above around 2900 m a.s.l., below this altitude wind direction changes from N winds to SE winds to S winds and finally to SW winds

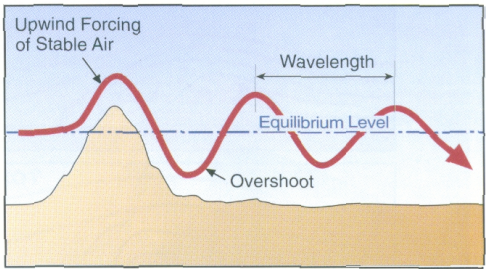

Figure 4.18: Lee waves are produced by stable stratified air that is lifted over mountains oscillating about its equilibrium on the lee side (figure taken from (Whiteman, 2000)).

from 5 pm to midnight. In the evening down-slope winds form, while valley wind is still present (Fig. 2.1). Down-slope winds might occur from Lauberhorn-Tschuggen range (N winds) and from Jungfrau, Mönch and Eiger range (SE to SSW winds).

Negative vertical velocity up to -1 ms^{-1} and winds from SE occurring from 4 pm to 6 pm might facilitate the decrease of the PBL height. The downdrafts ceases and light updrafts form, while the wind direction turns to SW after 6 pm, whereupon a second decreasing boundary layer height is observed. After 9 pm two residual layers are detected by the ceilometer.

During night vertical motion is poorly developed. In the morning strong updrafts are evident, increasing with height over daytime. Negative vertical velocity indicates the entrainment of air from free troposphere into the planetary boundary layer in the morning. This entrainment is an important factor for PBL growth. In the late afternoon a typical fair-weather cumulus cloud develops, resulting in downdrafts due to radiative cooling. Within the PBL the horizontal wind speed is rather week and the wind direction is not clearly defined compared to the wind direction above the PBL.

5 Conclusion

The investigation of the planetary boundary layer (PBL) was one research question of CLACE2010 (cloud and aerosol characterization experiment), which took place at the Kleine Scheidegg and at the Jungfraujoch (3580 m a.s.l.) in July and August 2010. Planetary boundary layer height was determined using the remote sensing instruments Jenoptik ceilometer CHM15k and Vaisala wind profiler LAP-3000 on eight fair-weather days during CLACE2010. These remote sensing instruments have been installed at the Kleine Scheidegg on 2061 m a.s.l.. The Kleine Scheidegg is in the vicinity of the Jungfraujoch within a distance of 4800 m.

To determine the PBL height using the ceilometer, the range corrected backscatter signal was used. A gradient method with and without thresholds were applied. The median of the maxima of the range corrected signal to noise ratio of each beam is used to identify PBL height over the Kleine Scheidegg. With the help of the wind profiler the planetary boundary layer height cannot be investigated at night (because turbulence is too weak) and during precipitation (cross sensitivity to falling hydrometers). The planetary boundary layer heights determined by ceilometer and wind profiler over daytime are in good agreement, especially during periods without clouds. Consequently, we can conclude that the aerosol layer height measured by the ground-based ceilometer seem to be consistent with the convective boundary layer height, which is detected by the ground-based wind profiler. This finding might be contrary to the results of the air-based remote sensing study coupled with simulations of de Wekker et al. (2004).

Unfortunately, it is not possible to determine from these data the height of stable boundary layer and of the planetary boundary layer during periods with clouds. An improvement of the PBL estimated by the wind profiler might by a combined analysis of vertical and radial velocity and maximum of range corrected signal-to-noise ratio. However, ceilometers are more appropriated for PBL analysis than a wind profiler, because they are able to identify residual layers at night and have a better vertical resolution.

The alpine planetary boundary layer is strongly influenced by mountain winds. Two successively decreasing layers are observed in the transition zone in the late afternoon. The appearance of these residual layers is explained by the influence of local winds with changing direction. Two decreasing residual layers are sometimes detected during night. They are interpreted as "historic layers" of the last few days. These two findings are also to some extend unexpected which are not mentioned in common literature (Stull, 1988; Garratt, 1992; Whiteman, 2000). Increasing

PBL height over a couple of fair-weather days (7 July - 12 July 2010), correspond with the findings of Lugauer (1998).

The relation between measured aerosol absorption and scattering coefficients at the Jungfraujoch and PBL height above the Kleine Scheidegg is not straightforward. Convective indifferent or advective weather types and a PBL height above 2800 m over the Kleine Scheidegg favor the observed PBL injections at the Jungfraujoch. Absorption and scattering coefficient peak in the afternoon and often high values are recorded during the evening. At the same time PBL height above the Kleine Scheidegg peaks around 1 pm and decreases after 4 pm. In conclusion, updraft winds transport injections of the PBL to the Jungfraujoch, where they are measured with a time delay of a few hours. This air mass persists at the Jungfraujoch until it is replaced by free troposphere air in the late night. In addition, absorption and scattering coefficient are also controlled by pollutant concentration and photochemical processes in the free troposphere. Besides, advection of aerosol and Sahara dust influences the measurement values and hamper the correlation with the remote sensing derived PBL above the Kleine Scheidegg.

As the correlation between simulated PBL height determined by COSMO-2 and determined by the remote sensing instruments at the Kleine Scheidegg is weak, further investigations of the numerical model are necessary. Improvement of the input parameters and probably an adjustment of the method might lead to better results. Furthermore, the simulations might improve using observations. However, no continuously operating measuring instruments, which detect PBL height automatically, are installed in the Alps. Despite of the good agreement between PBL determined by wind profiler and ceilometer I would recommend to use PBL derived by ceilometers, as they measure aerosol layer heights, for comparison with COSMO-2 PBL. Furthermore, ceilometers have the advantage, that they can be used to determine the residual layers at night.

Bibliography

Angevine, W. M., A. B. White, S. K. Avery, 1994: Boundary-layer depth and entrainment zone characterization with a boundary-layer profiler. Boundary-Layer Meteorology, 68(4), p. 375-385

Angevine, W. M., P. Barkwin, K. J. Davis, 1997: Wind profiler and RASS measurements compared with measurements from a 450-m-tall tower. Journal of Atmospheric and Oceanic Technology, 15, p. 818-825

Barry, R., 2005: Mountain weather and climate. Cambridge University Press. Cambridge. 3. edition 512 pp.

Barry, R., R. Chorley, 2003: Atmosphere, weather and climate. Routledge. London and New York. 8. edition 462 pp.

Bendix, J., 2004: Geländeklimatologie. Berlin, Stuttgart: Geb. Bornträger Verlagsbuchhandlung. 282 pp.

Beyrich, F., J. Bange, U. Görsdorf, O. Hartogensis, S. Martin, 2010: Cross validation of boundary-layer parameters from in-situ measurements and ground-based remote sensing. 15th International Symposium for the Advancement of Boundary Layer Remote Sensing (ISARS). 28-30 June 2010. Paris.

Bianco, L., J. Wilczak, 2002: Convective Boundary Layer Depth: Improved measurement by Doppler wind profiler using fuzzy logic method. Journal of Atmospheric and Oceanic Technology, 19, p. 1745-1758

Brunekreef, B. and S. Holgate, 2002: Air pollution and health. The Lancet, 360, 9341, p. 1233-1242

Collaud Coen, M., E. Weingartner, A. Apituley, D. Ceburnis, R. Fierz-Schmidhauser, H. Flentje, J. S. Henzing, S. Jennings, M. Moerman, A. Petzold, O. Schmid and U. Baltensperger, 2010: Minimizing light absorption measurement artifacts of the Aethalometer: evaluation of five correction algorithms. Atmospheric Measurement Techniques, 3, p. 457-475

Collaud Coen, M., E. Weingartner, M. Furger, S. Nyeki, A. Prévôt,S. Steinbacher and U. Baltensperger, 2011: Planetary boundary influence at the Jungfraujoch analyzed by aerosol cycles and synoptic weather types. Atmospheric Measurement Techniques, 11, p. 5931–5944

COST Action 76, 2001: Development of VHF/UHF wind profilers and vertical sounders for use in European observing system. Editor, J. Dibbern. COST action 76. Final report, November 2001. Office for Official Publications of the European Communities, Luxembourg. 433 pp.

Defant, F., 1951: Local winds. Compendium of Meteorology. Editor, T. F. Malone. American Meteorological Society, p. 655-672

Emeis, S., K. Schäfer, C. Münkel, 2006: Surface-based remote sensing of the mixing-layer height-a review. Meteorologische Zeitschrift, 17(5), p. 621-630

Fierz-Schmidhauser, R., P. Zieger, M. Gysel, L. Kammermann, P. F. DeCarlo, U. Baltensperger and E. Weingartner, 2010: Measured and predicted aerosol light scattering enhancement factors at the high alpine site Jungfraujoch. Atmospheric Chemistry and Physics, 10, p. 2319-2333

Flentje, H., J. Reichardt and W. Thomas, 2009: Aerosol profiling using DWD's ceilometer network. GAW Letter of DWD, 49, 2 pp. (http://www.dwd.de/gaw)

Flentje. H., H. Claude, T. Elste, S. Gilge, U. Köhler, C. Plass-Dülmer, W. Steinbrecht, W. Thomas, A. Werner, and W. Fricke, 2010a: The Eyjafjallajökull eruption in April 2010 - detection of volcanic plume using in-situ measurements, ozone sondes and lidar-ceilometer profiles. Atmospheric Chemistry and Physics, 10, p. 10085-10092

Flentje, H., B. Heese, J. Reichardt, and W. Thomas, 2010: Aerosol profiling using the ceilometer network of the German Meteorological Service. Atmospheric Measurement Techniques, Discussion, 3, p. 3643-3673

Frey, S., K. Poenitz, G. Teschke, H. Wille, 2010: Detection of aerosol layers with ceilometers and the recognition of the mixed layer depth. International Symposium for the advancement of boundary layer remote sensing. 28.-30.06.2010. Paris.

Gaffard, C., L. Bianco, M. Matabuena, V. Klaus, 2005: Toward the estimation of the refractive index gradient from clear air wind profiler echoes. 13th Symposium on Meteorological Observations and Instrumentation. Savannah, USA. 14 pp.

Garratt, J. R., 1992: The atmospheric boundary layer. Cambrige University Press. Cambridge. 316 pp.

Grimsdell, A. and W. Angevine, 1998: Convective boundary layer height measurement with wind profilers and comparison to cloud base. Journal of Atmospheric and Oceanic Technology, 15, p. 1331–1338

Haeffelin, M., Y. Morille, F. Angelini, S. Frey, S. Lolli, G. Martucci, L. Sauvage, G. Teschke, 2009: Retrieval of mixing layer depth from existing ceilometer/lidar networks in Europe. ICOS AS workshop Gif/Yvette, 23-24.11.2009.

Haij, M., W. Wauben and H. Klein Baltink 2007: Continuous mixing layer height determination using the LD-40 ceilometer: a feasibility study. KNMI. De Bilt. 98 pp.

Hammer, E., 2011: Calculation and Interpretation of cloud peak supersaturation at the Jungfraujoch. Masterthesis. University of Bern. 52 pp.

Hansen, A., 2005; The Aethalometer. Magee Scientific Company. Berkeley, California, USA. 210 pp.

Hatzianastassiou, N., C. Matsoukas, E. Drakakis, P. Stackhouse Jr., P. Koepke, A. Fotiadi, K. Pavlakis, and I. Vardavas, 2007: The direct effect of aerosols on solar radiation based on satellite observations, reanalysis datasets, and spectral aerosol optical properties from Global Aerosol Data Set (GADS). Atmospheric Chemistry and Physics, 7, p. 2585-2599

Heese, B., H. Flentje, D. Althausen, A. Ansmann and S. Frey, 2010: Ceilometer lidar comparison: backscatter coefficient retrieval and signal-to-noise ratio determination. Journal of Atmospheric and Oceanic Technology, 3, p. 1763-1770

Henne, S., M. Furger and A. Prévôt, 2005: Climatology of mountain venting-induced elevated moisture layers in the lee of the Alps. Journal of Applied Meteorology, 44, p. 620-633

Hennemuth, B. and A. Lammert,2006: Determination of the atmospheric boundary layer height from radiosonde and lidar backscatter. Boundary-Layer Meteorology, 120, p. 181-200

TSI,2001: Instruction Manual. Model3936 SMPS (Scanning Mobility Particle Sizer). 83 pp.

IPCC, 2007: Climate Change 2007: The Physical Science Basis. Contribution of Working Group I to the Fourth Assessment Report of the Intergovernmental Panel on Climate Change (Solomon, S., D. Qin, M. Manning, Z. Chen, M. Marquis, K.B. Averyt, M. Tignor and H.L. Miller (eds.). Cambridge University Press, Cambridge and New York. 996 pp.

Jaenicke, R., 1992: Nucleation and atmospheric aerosol. Ed. N. Fukuta and Wagner, P., Deepack Publication, Hampton, Virginia, 117 pp.

James, P. K., 1980: A review of radar observations of the troposphere in clear air conditions. Radio Science, 15(2), p. 151-175

Jenoptik, 2009: CHM 15 K / CHM 15-kx Wolkenhöhenmessgerät (Ceilometer). Bedienerhandbuch. Jena. 73 pp.

Kossman, M., 1999: Observation of handover processes between the atmospheric boundary layer and the free troposphere over mountainous terrain. Contributions to Atmospheric Physics, 72, p. 329-350

Kossman, M., 1998: Aspects of the convective boundary layer structure over complex terrain. Atmospheric Environment, 32(7), p. 1323-1348

Lee, S. J. and H. Kawai, 2011: Mixing depth estimation from operational JMA and KMA windprofiler data and its preliminary applications: examples from four selected sites. Journal of the Meteorological Society of Japan, 89(1), p. 15-28

Lehtinen, R., R. Shellhorn, A. Lilja, 2009: New wind profiling algorithms from Vaisala. In: Proceedings of the 8th International Symposium on Tropospheric Profiling. Editors, A. Apituley, H. Russchenberg, W. Monna. Delft, The Netherlands. 3 pp.

Lugauer, M., U. Baltensperger, M. Furger, H. Gäggeler, D. Jost, S. Nyeki, M. Schwikowski, 2000: Influences of vertical transport and scavening on aerosol particle surface area and radon decay product concentrations at the Jungfraujoch (3454 m above sea level). Journal of Geophysical Reasearch, 105, D15, p. 19,869 - 19,879

Lugauer, M., U. Baltensperger, M. Furger, H.W. Gaggeler, D.T. Jost, M. Schwikowski, and H. Wanner, 1998: Aerosol transport to the high alpine sites Jungfraujoch (3454 m asl) and Colle Gnifetti (4452 m asl). Tellus, 508, p. 76-92

Lugauer, M., 1998: Vertical transport of atmospheric trace species in the Alps. Dissertation. Bern.

Morille, Y., M. Haeffelin, P. Drobinski and J. Pelon, 2006: STRAT: An automated algorithm to retrieve the vertical structure of the atmosphere from single-channel lidar data. Journal of atmospheric and oceanic technology, 24, p. 761-775

Nyeki, S., U. Baltensperger, I.Colbeck, D.T. Jost, E. Weingartner, and H. W. Gäggeler, 1998: The Jungfraujoch high-alpine research station (3454 m) as a background clean continental site for the measurement of aerosol parameters. Journal of Geophysical research, 193(D6), p. 6097-6107

Nyeki, S., M. Kalberer, I.Colbeck, S. de Wekker, M. Furger, H. G¨aggeler, M. Kossmann, M. Lugauer, D. Steyn, E. Weingartner, M. Wirth, and U. Baltensperger, 2000: Convective boundary Layer Evolution to 4 km asl over High-Alpine Terrain: Airborne Lidar Observations in the Alps. Geophysical Research Letters, 27(5), p. 698-692

Nyeki, S., K. Eleftheriadis, U. Baltensperger, I. Colbeck, M. Fiebig, A. Fix, C. Kiemle, M. Lazaridis, and A. Petzold, 2002: Airborne Lidar and in-situ Aerosol Observations of an Elevated layer, leeward of the European Alps and Apennines. Geophysical Research Letters, 29(17), p. 33-1 - 33-4

Pino, D, 2011: Boundary layer late afternoon and sunset turbulence. Presentation at Special Working Group Meeting of Eg-CLIMET COST ACTION. Palaiseau. April 2011.

Ruffieux, D. and R. Stübi, 2001: Wind profiler as a tool to check the ability of two NWP models to forecast winds above highly complex topography. Meteorologische Zeitschrift, 10(6), p. 489-495

Schüepp, M., 1979: Witterungsklimatologie, Klimatologie der Schweiz, Band III, Beilage zu den Annalen 1978, MeteoSwiss, Zürich, Switzerland.

Seibert,P., F. Beyrich, S.-E. Gryning, S. Joffre, A. Rasmussen, P. Tercier, 2000: Review and intercomparison of operational methods for the determination of the mixing height. Atmospheric Environment, 34, p. 1001-1027

Seinfeld, J. H., Pandis, S. N., 2006: Amtospheric chemistry and physics. From air pollution to climate change. John Wiley and Sons, Inc., Hoboken, New Jersey, 2nd edition. 1248 pp.

Stull, R. B., 1988: An introduction to boundary layer meteorology. Kluwer Academic Publlisher. AH Dordrecht. 666 pp.

Teschke, G. and K. Poenitz, 2010: On the retrieval of aerosol (mixing) layer heights on the basis of ceilometer data. International Symposium for the Advancement of Boundary Layer Remote Sensing. 28.-30.06.2010. Paris.

Vogelezang, D. and A. Holtslag, 1996: Evaluation and model impacts of alternative boundary-layer height formulations. Boundary-Layer Meteorology 81, p. 245-269

Vaisala, 2007b: Software Manuel LAP XM Rev. 2.4.1.0. Technical Reference. 225 pp.

Vaisala, 2007a: Vaisala wind profiler. User's Guide. 217 pp.

Wallace, J. M. and P. V. Hobbs, 2006: Atmospheric science. An introductory survey. Academic Press. London. 480 pp.

Weigel, A., 2005: On the atmospheric boundary layer over highly complex topography. Dissertation, ETH No 15972. 155 pp.

Weingartner, E., H. Saathoff, M. Schnaiter, N. Streit, B. Bitnar, U. Baltensperger, 2003: Absorption of light by soot particles: determination of the absorption coefficient by means of aethalometers. Journal of Aerosol Science, 34, p. 1455-1463

Weitkamp, C., 2005: Lidar. Range-resolved optical remote sensing of the atmosphere. Springer Science. 455 pp.

Whiteman, C.D., 2000: Mountain meteorology. Fundamentals and applications. Oxford University Press. New York. Oxford. 355 pp.

Wilczak, J., R. Strauch, F. Ralph, B. Weber, J. Jordan, D. Wolfe, L. Lewis, D. Wuerst, J. Gaynor, S.A. McLaughlin, R. Rogers, A. Riddle, T. Dye, 1995: Contamination of wind profiler data by migrating birds: characteristics of corrupted data and potential solutions. Journal of Atmospheric and Oceanic Technology, 12, p. 449–467

de Wekker, S., D. Steyn and S. Nyeki, 2004: A comparison of aerosol layer and convective boundary layer structure over mountain range during STAARTE. Boundary Meteorology 113, p. 249-271

de Wekker, S., 2002: Structure and morphology of the convective boundary layer in mountainous terrain. Dissertation. The University of British Columbia. Canada. 191 pp.

Wetzel, P., 1982: Toward parameterization of the stable boundary layer. Journal of Applied Meteorology 21, p. 7-13

York, D., N. Evensen, M. Lopez Martinez and J. De Basabe Delgado, 2004: Unified equations for the slope, intercept, and standard errors of the best straight line. American Journal of Physics, 72(3), p. 367-375

Acknowledgment

This project would not have been possible without the help of various people. That is why I wish to mention some people who supported me during this project.
Paul Zieger was always able to answer my various questions and to give helpful input.
I want to thank Ernest Weingartner, Nikolas Buckowieski, Martin Gysel and Margit Schwikowski for their help and ideas.
Martine Collaud-Coen and Dominique Ruffieux, thank you for your inputs and the discussions.
Furthermore, I want to thank Emanuel Hammer for explaining all aerosol measurement instruments at the Jungfraujoch and Markus Furger for the discussions about mountain meteorology.

Declaration

under Art. 28 Para. 2 RSL 05

Last, first name: Ketterer,Christine

Matriculation number: 09-121-344

Programme: Climate Sciences

Master

Thesis title: Investigation of the planetary boundary layer using remote sensing and in-situ measurements at the Kleine Scheidegg and at the Jungfraujoch

Thesis supervisor: Prof. Dr. Margit Schwikowski

Dr. Ernest Weingartner

I hereby declare that this submission is my own work and that, to the best of my knowledge and belief, it contains no material previously published or written by another person, except where due acknowledgement has been made in the text. In accordance with academic rules and ethical conduct, I have fully cited and referenced all material and results that are not original to this work. I am well aware of the fact that, on the basis of Article 36 Paragraph 1 Letter o of the University Law of 5 September 1996, the Senate is entitled to deny the title awarded on the basis of this work if proven otherwise.

Villigen, 12 December 2011

Christine Ketterer

Signature